

CLICK-CHEMISTRY BASED MOLECULARLY RESPONSIVE HYDROGELS AS
BIODEGRADABLE SCAFFOLDS FOR 3-D CELL CULTURE: DESIGN AND
PREPARATION OF BUILDING BLOCKS

By

Renato Navarro, B.S.

A thesis submitted to the Graduate Council of
Texas State University in partial fulfillment
of the requirements for the degree of
Master of Science
with a Major in Chemistry
August 2014

Committee Members:

Tania Betancourt, Chair

Corina Maeder

William Brittain

Copyright Page

By

Renato S. Navarro

2014

FAIR USE AND AUTHOR'S PERMISSION STATEMENT

Fair Use

This work is protected by the Copyright Laws of the United States (Public Law 94-553, section 107). Consistent with fair use as defined in the Copyright Laws, brief quotations from this material are allowed with proper acknowledgment. Use of this material for financial gain without the author's express written permission is not allowed.

Duplication Permission

As the copyright holder of this work I, Renato S. Navarro, authorize duplication of this work, in whole or in part, for educational or scholarly purposes only.

DEDICATION

This work is dedicated to my daughter Izabela B. Navarro.

ACKNOWLEDGEMENTS

This work could not have been accomplished without the support and mentorship that I have received through out my life, from teachers, friends, and even drill sergeants. Although it is impossible to name everyone here, I would like to take a few lines to thank those that have influenced my career and life the most.

I would like to start by thanking Dr. Tania Betancourt for all the support, mentorship, and conversations these last two years. It has definitely been a journey, you have pushed me to be better in all aspects of my life and have put up with me when I failed. I owe you a debt of gratitude that words aren't able to express so I hope that through my continued success I can convey to you the gratitude and appreciation that I have for all that you have given me. I hope that one-day I can show you that the time and support you have shown me were well spent. Thank you. I would also like to thank my lab mates Travis Cantu and Robert Danso for their help, support, and friendship these last two years. I would also like to thank the undergrads who I mentored and helped to make this work possible: Katie Beaven, Kole Knutson, Ronald Hall, and Jamie McKinzie. The friends I have made at Texas State University deserve a big thank you as well; you guys were there through those long days and I couldn't have done it with out you. To the CHB club, I know it has been a long time, but know that I hold each of you dearly in my heart. I will always cherish your friendship and I hope one day it could be like the good old days.

I would also like to thank my committee member Dr. Corina Maeder and Dr. William Brittain. Your input and mentorship thorough out the last two years has been appreciated and invaluable. Lastly, I would also like to thank Dr. Shiva Rastogi. You taught me more chemistry in two months than I learned in my undergrad. Thank you all.

TABLE OF CONTENTS

	Page
ACKNOWLEDGEMENTS	v
LIST OF TABLES	ix
LIST OF FIGURES	x
LIST OF EQUATIONS	xii
ABSTRACT	xiii
CHAPTER	
1. INTRODUCTION AND BACKGROUND	1
1.1. Significance and approach	1
1.2. Hydrogel	6
1.3. POLY(ethylene glycol).....	9
1.4. Aptamers.....	12
1.5. Systematic evolution of ligands by exponential enrichment	15
1.6. Vascular endothelial growth factor	17
1.7. Copper-free click chemistry.....	18
2. DESIGN AND EVALUATION OF APTAMER COMPLEX.....	22
2.1. Melting temperature simulation for DNA complex.....	24
2.1.1. Materials and methods	26
2.1.2. Results and discussions.....	27
2.2. Monitoring of system 1 and system 2 complex formation via fluorescence	33
2.2.1. Materials and methods	33
2.2.2. Results and discussions.....	35
2.3. Temperature dependence of system 1 and system 2	40
2.3.1. Materials and methods	41
2.3.2. Results and discussions.....	41
2.4. System 2 response to VEGF	43
2.4.1. Materials and methods	43

2.4.2. Results and discussions.....	43
3. HYDROGEL SYNTHESIS USING PEG CROSSLINKER.....	46
3.1. DBCO synthesis.....	46
3.1.1. Materials and methods.....	46
3.1.2. Results and discussions.....	49
3.2. PEG-DBCO conjugation.....	50
3.2.1. Materials and methods.....	51
3.2.2. Results and discussions.....	53
3.3. Hydrogel Synthesis.....	54
3.3.1. Materials and methods.....	54
3.3.2. Results and discussions.....	55
4. CELL ADHESIVE PEPTIDE.....	57
4.1. Cyclo arginine glycine aspartic acid synthesis.....	57
4.1.1. Materials and methods.....	58
4.1.2. Results and discussions.....	59
5. SUMMARY AND CONCLUSIONS.....	61
REFERENCES.....	63

LIST OF TABLES

Table	Page
1. Fit Parameters for equation 2	24
2. Monovalent and divalent salt concentrations used to determine T_m	27
3. Buffer concentrations used in quenching study for Systems 1 and 2	35

LIST OF FIGURES

Figure	Page
1. Hydrogel synthesis schematic.....	4
2. Copolymer formulation.....	9
3. Poly(ethylene glycol) synthesis	10
4. Polymer configurations.....	11
5. PEGylation of various macromolecules.....	11
6. Aptamer complex variations and degradation	14
7. VEGF aptamer tertiary structure and VEGF interaction	15
8. Schematic of SELEX process	16
9. VEGF protein.....	18
10. Schematic of copper-catalyzed click chemistry reaction.....	19
11. Schematic of copper-free click chemistry reaction.....	20
12. Design of aptamer complex	25
13. Melting temperature of (A) strand Q and (B) F of System 1 (S1).....	29
14. Melting temperature of (A) strand Q and (B) F of System 2 (S2).....	32
15. Quenching of System 1 (S1) at various NaCl concentration	37
16. Quenching of System 2.....	40
17. Temperature response of System 2	42
18. Aptamer complex response to VEGF	45

19. Step one of DBCO synthesis.....	47
20. Step two of DBCO synthesis	48
21. Step three of DBCO synthesis	48
22. Step four of DBCO synthesis.....	49
23. Step five of DBCO synthesis	49
24. DBCO UV-vis absorption.....	50
25. Carbon-13 NMR of DBCO molecule	51
26. DBCO addition to PEG-NH ₂	52
27. Absorption spectra of PEG-DBCO.....	53
28. Experimentally derived proton NMR spectra of PEG-DBCO.....	54
29. Hydrogel synthesis using PEG-Azide substitute crosslinker.....	56
30. Structure of cRGD peptide.....	57
31. MALDI-TOF spectrum of cRGD peptide.....	60

LIST OF EQUATIONS

Table	Page
1. Sodium dependent equation	23
2. Magnesium dependent equation	23

ABSTRACT

According to the American Cancer Society, every year over one million Americans are diagnosed with one of the recognized forms of cancer. Cancer metastasis is associated with poor patient prognosis. In order to better understand how cancer grows and metastasizes, researchers are interested in the development of platforms that could model the environment of tumor tissue and enable the study of the effect of cancer cell-secreted molecules on cell replication, extracellular matrix remodeling, and cell migration leading to metastasis. Due to their tissue-like properties, hydrogels have the ability to serve as such model systems by providing a three-dimensional scaffold in which cancerous cells could be cultured and studied. Hydrogels are formed from physically or chemically cross-linked hydrophilic polymers that form insoluble networks. Due to their high water content, hydrogels have mechanical properties that are similar to those of tissue; therefore, hydrogels could become ideal platforms for the study of cell growth and migration.

The long-term goal of this work is to develop a hydrogel system that is molecularly responsive and can be synthesized at physiological conditions that could be used as a model the study of cancer cell growth. In order to achieve this goal, in this work we focused on: (1) the development of an aptamer complex to be used as crosslinker within the hydrogel network that is responsive towards the cancer cell-secreted protein vascular endothelium growth factor (VEGF), (2) the development of methods for the synthesis of

hydrogels under mild conditions via copper-free click chemistry, and (3) the integration of cell adhesive properties to the hydrogels through a cyclo-Arginine-Glycine-Aspartic Acid (cRGD) peptide that mimics fibrin and collagen, some of the most abundant protein components of the extracellular matrix. The aptamer complex was designed to be able to hybridize at physiological conditions but denature in the presence of the molecular target VEGF, yielding a system that is responsive and degradable. Through the use of copper-free click chemistry, the hydrogels could be synthesized in the absence of toxins like free radicals, metals, and ultraviolet light that are typically used in polymerization reactions but that have deleterious effects on cells. The bioorthogonal reaction between azide and dibenzylcyclooctyne utilized in the copper-free click chemistry reaction is able to rapidly link polymeric precursors, thus providing a method for immediate the encapsulation of cancer cells within the hydrogel scaffold. The encapsulated cells are then able to interact with the mimicry peptide cRGD and signal the cells to begin growing and proliferating. In doing so, a hydrogel that is molecular responsive, nontoxic, and capable of encapsulating cells is fashioned in order to serve as three-dimensional platform for their study.

Chapter 1 provides a background on the various concepts on which the proposed biomaterial design is based. Chapter 2 discusses the design and *in vitro* evaluation of VEGF-responsive aptamer complexes to be used in later work as crosslinkers of molecularly controlled biodegradable hydrogels. Chapter 3 describes the work that was performed for the development of synthetic protocols to be used for the preparation of the

hydrogels using click chemistry. Chapter 4 describes the methods used for solid-phase synthesis of the mimicry peptide cRGD. Finally, Chapter 5 summarizes the work and provides concluding remarks.

1. INTRODUCTION AND BACKGROUND

1.1. SIGNIFICANCE AND APPROACH

The human body is a complex system that has the ability to heal and regenerate itself; however, after a traumatic injury or disease our bodies lose the ability to carry out regeneration and healing [6-8]. Learning how cells are able to regenerate or heal themselves, and how tissues undergo changes under pathological conditions are topics that have been of interest to researchers. Methods using hydrogels as platforms to facilitate the growth and regeneration have been developed to study these processes both *in vivo* and *in vitro* [9-14]. The ability to isolate a particular cell type and create a microenvironment that mimics the tissue in which it naturally inhabits is of particular interest to researchers.

Much work has gone into creating polymeric scaffolds that are able to closely mimic these physiological environments [15, 16]. Similarly, scaffolds have been created to study how cancerous cells grow, proliferate, and metastasize [17]. These scaffolds or matrices have been of interest because they are able to provide environments that closely match tissues, which the cancer occupies, while also providing sufficient environmental control for the study of relevant pathological processes such as growth factor secretion, cell replication, and cell migration. This has led to the development of platforms that are used to test cellular response to drug delivery systems, evaluate drug toxicity, as well as study how cancer metastasizes *in vitro* and *in vivo* [18-20]. Although, two-dimensional and three-dimensional polymeric scaffolds have been developed and implemented in studying cancer cell behavior and growth, we believe that there is room for improvement in the

design of current systems in use. Three-dimensional scaffolds have the advantage over two-dimensional scaffolds of better mimicking the environment that cells occupy in the body and have become the “gold standard” and therefore provide the best platform for our intended use [8, 16, 17]. Our approach is to create a biodegradable hydrogel from synthetic polymers to act as a scaffold for the study of cancer cells in culture. This scaffold will not only provide the initial support system in which cells can grow and proliferate, but will also be able to degrade in response to molecular cues from the cancerous cells. This will allow the degradation of the scaffold to match growth and proliferation of the cells, and will provide a means for the study of the role of cell-secreted molecules on cell replication, migration, and extracellular matrix remodeling.

The long-term objective of the work commenced here is to develop a hydrogel-based biomaterial that can specifically interact with molecular targets and provide a response (disintegration) as a consequence of this interaction. This new type of biomaterial, if prepared and utilized under biologically relevant conditions, could be used as a scaffold for the study of cancer cell growth. The work presented in this thesis focuses on: (1) development and evaluation of DNA-based aptamer complexes as molecularly responsive crosslinkers of hydrogel networks (Chapter 2), (2) the development of synthetic methods for the preparation of the hydrogels via copper-free click chemistry (Chapter 3), and the preparation of peptide mimics of the extracellular matrix for incorporation into the hydrogel to encourage cell attachment and growth (Chapter 4). The aptamer complex is the key feature that can provide the hydrogel molecular responsiveness. As will be discussed later, it is designed so that it is stable in the hybridized form at physiological conditions but can be induced to dehybridize upon

interaction with the molecular target, thus effectively providing a means for molecularly controlled crosslinker dissociation. In addition to the work herein presented, efforts are focusing on the integration of cell adhesive peptides based on cyclo-Arginine-Glycine-Aspartic Acid (cRGD) that mimic fibrin and collagen, some of the most abundant proteinic components of the extracellular matrix to provide more biocompatibility to the biomaterial.

Figure 1 depicts the design and envisioned function of the proposed molecularly responsive hydrogel scaffolds, and three major steps required to prepare them. Starting with Figure 1A, a four-arm 20,000 Da molecular weight (MW) poly(ethylene glycol) (PEG) is end functionalized with dibenzylcyclooctyne (DBCO). Following the functionalization of the PEG, the synthesis of the hydrogel can be carried out as shown in Figure 1B. This step involves incorporating the functionalized four-arm PEG, cRGD that has been conjugated to a 5,000 Da MW PEG that is azide functionalized, cancer cells (here represented by human SKOV-3 ovarian cancer cells), and the aptamer complex that has been azide functionalized. As shown in the figure, the azide groups (represented by triangles on Figure 1A) and the DBCO end groups on PEG react to form a covalently linked network. This critical step will form the aptamer crosslinked hydrogel with cells encapsulated within (Figure 1C). The use of copper-free click chemistry ensures that the reaction can be conducted at 37 °C (physiological temperature) without the use of catalyst or free radicals that are detrimental to cells.

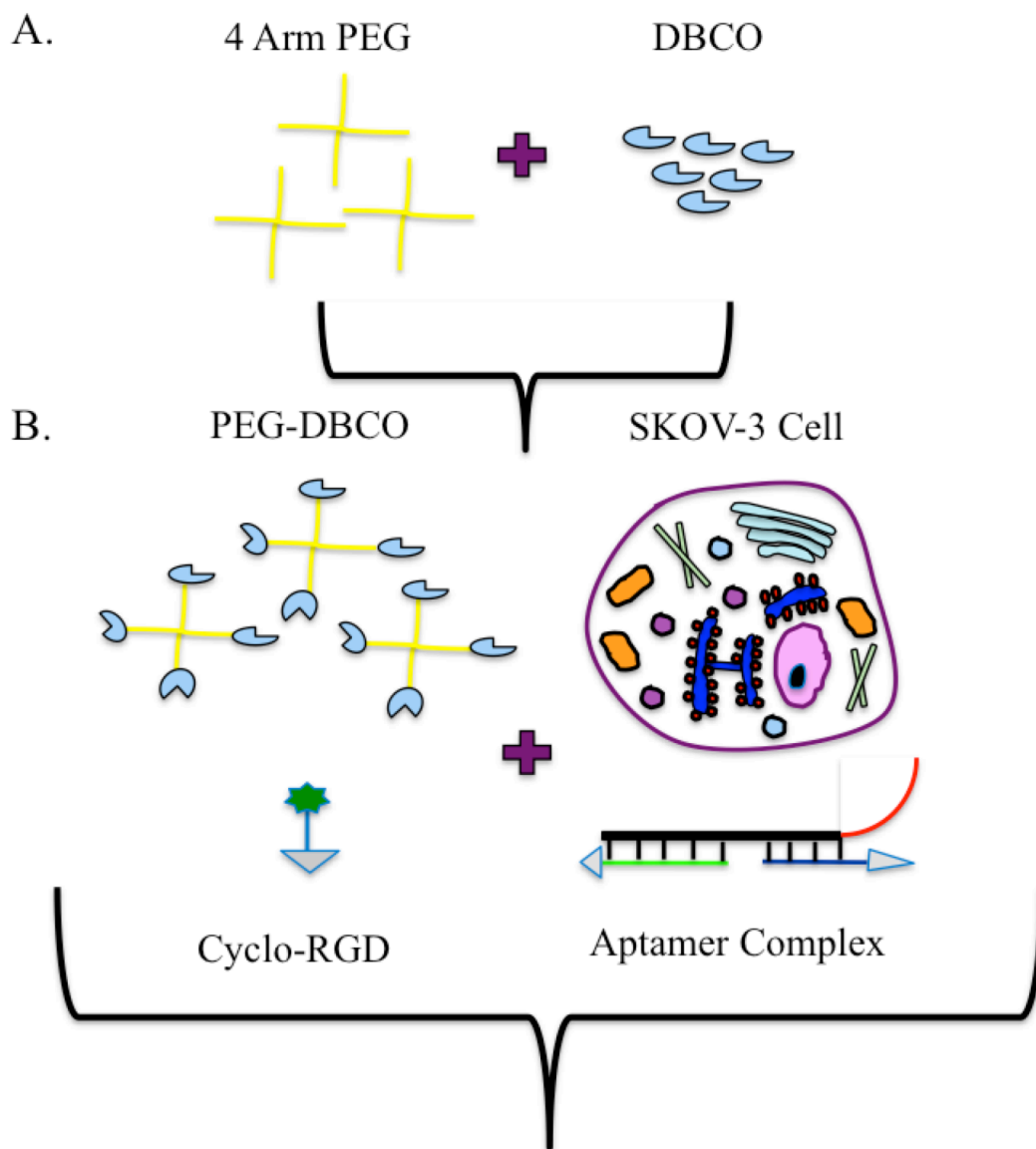


FIGURE 1. Hydrogel synthesis schematic **A)** Hydrogel synthesis starting with 4-arm PEG being end functionalized with DBCO. **B)** One-pot synthesis of hydrogels incorporating SKOV-3 cancer cells, cRGD, aptamer complex, and four-arm PEG-DBCO. **C)** Inset showing hydrogel with adhered cells that are secreting VEGF protein and the design of the aptamer complex. This complex consists of three oligonucleotide strands (here presented in green, blue, and black/red), one of which contains the VEGF-specific aptamer (red). As the VEGF protein makes contact with the aptamer in the aptamer complex, it competitively displaces one of the complementary strands (blue), thus disrupting the hydrogel crosslinks and enabling degradation of the hydrogel. Figure 1 continued

C.

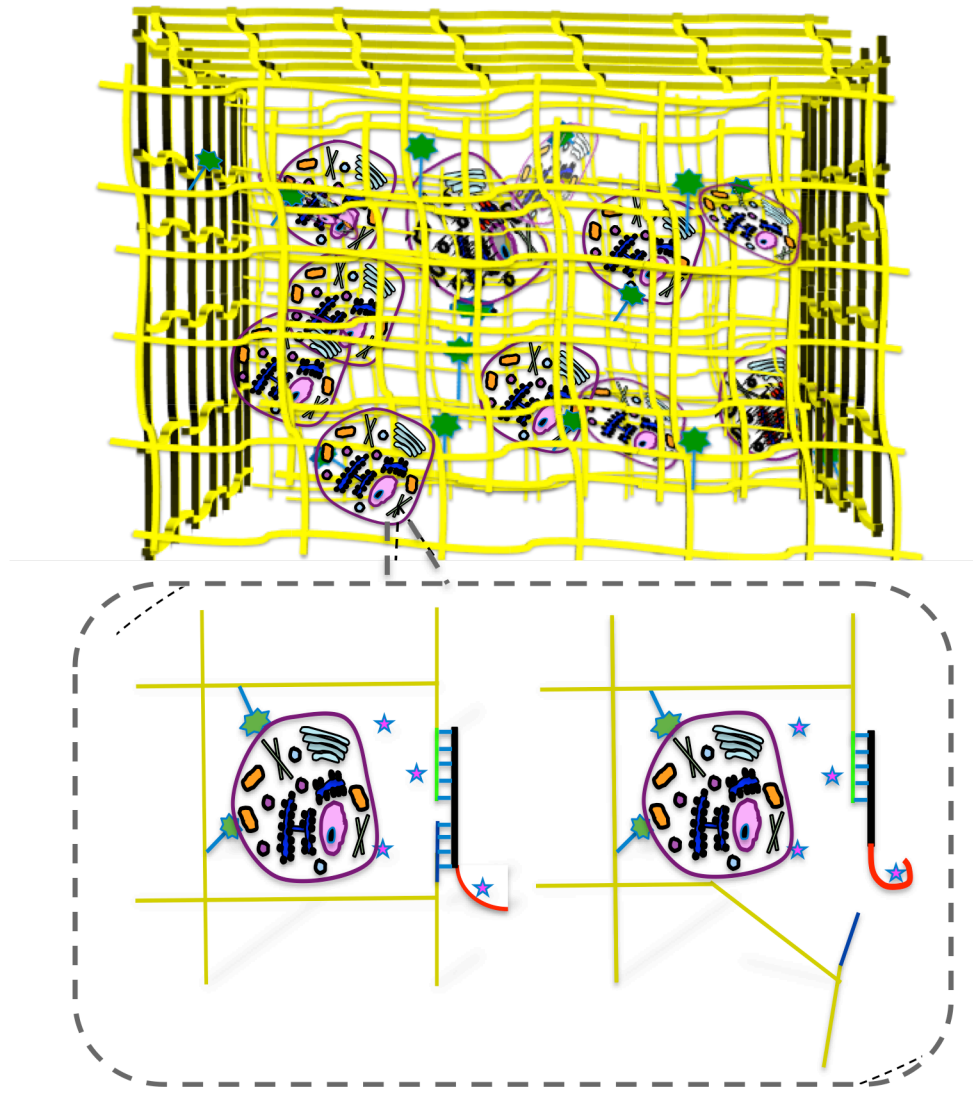


Figure 1 continued.

Figure 1C shows how the cells will randomly distribute within the matrix and adhere to the cRGD molecular anchors via integrins, which are cell surface receptors that typically participate on cell-cell and cell-extra cellular matrix adhesion. As the cells begin to grow and proliferate within the hydrogel, the area around them will become hypoxic and trigger the cells to begin secreting the vascular endothelial growth factor (VEGF) protein [18, 19]. The secreted protein will interact with the aptamer on the crosslinker complex. The interaction between the VEGF protein and the aptamer is based on the large number of protein molecules secreted into the interstitial fluid and the aptamers' affinity for the VEGF protein. When this binding occurs, the protein causes a change in the aptamers' three-dimensional structure. The change in conformation allows the aptamer to bind to the VEGF protein with higher affinity than to the partially complementary strand, thus allowing the complex to completely dissociate (blue strand displacement in Figure 3C). Through the dissociation of the complementary strands that make up the aptamer complex crosslinker, we are able integrate degradability and molecular responsiveness into the hydrogel.

1.2. HYDROGEL

Hydrogels were first described by Wichterle and Lim in 1954 [4]. The hydrogels first described and characterized by Lim were of interest to researchers because they were able to create an amorphous polymer network that was insoluble and unable to form crystalline states. The networks described were able to encapsulate copious amounts of water with low polymer weight to volume (w/v) percent. These networks with low mechanical properties and tissue-like characteristics paved the way for their incorporation in the next 60 years to numerous medical applications. Since then, hydrogels have been

used in biomedical/bioengineering for functions that range from drug delivery systems [19, 21-24], contact lenses [25-27], and tissue engineering [6, 28-32]. Today the definition of a hydrogel has been largely broadened to hydrophilic polymers that are either chemically or physically crosslinked. The formation of the hydrogel is not necessarily dependent on covalent bonds between polymers or through the use of chemical crosslinker molecules used to anneal the chains together. Hydrogel synthesis has expanded to include networks that are held together by non-covalent interactions such as those that incorporate crystalline regions, or are held together by ionic interaction or hydrogen bonds. One conserved characteristic from the hydrogels first described by Lim and Wichterle that has remained true through out these 60 years is the ability of the hydrophilic polymers to encapsulate large volumes of water resulting in network swelling.

The broadening of the hydrogel definition can be attributed to expanding the hydrophilic polymers and crosslinker used in hydrogel synthesis today. Primarily the quantity and quality of hydrophilic polymers has expanded from methacrylates used by Lim to include newer synthetic polymers and biomolecules. The formulation of hydrogel now includes natural polymers derived from amino acids [33-35], carbohydrates [36-39], and nucleic acids [40, 41] that are able to interact favorably with other biomolecules. The amounts of synthetic polymers have also grown as newer and more suitable polymers are developed to interface with biological systems [42-47]. Although diminished toxicity is a purpose in mind when designing synthetic polymers, in the last twenty years polymers have been developed that allow responsiveness to pH [48-54], temperature [55-59], and degradation due to hydrolysis [60-64]. Similarly, crosslinkers, molecules that anneal

polymer strands chemically or physically together, can be made from either synthetic or natural polymers [65, 66].

By combining two or more of the polymers and forming a copolymer, as shown in Figure 2, copolymers with varying functionalities can be synthesized. The ratio in which the monomers or polymers are used to synthesize the resulting copolymer will have significant impact in how the polymer behaves. For example if the goal is to create a degradable hydrogel, incorporation of larger ratios of degradable polymer compared to nondegradable one when forming a copolymer will cause the copolymer to degrade faster than if they were in even proportions. Being that the main aim of this project entails the formation of a “smart” hydrogel that is degradable and responsive to molecular cues, the polymer that was used in this work consist of a block copolymer formed from PEG and DNA. Specifically, and compared to previously reported biodegradable hydrogels [67-75], the hydrogel that is being synthesized incorporates a responsive crosslinker complex made from DNA that will dissociate in order to provide molecularly controlled degradability to the network. The inclusion of natural polymers has been mainly investigated in order to achieve effective matrix-cellular interactions that are crucial in the formation of tissue culture microenvironments [15, 76-79]. Most recently biopolymers have been designed to respond similarly to environmental stimuli including temperature [80-83], salt concentrations [84-87], and pH [84, 87-89].

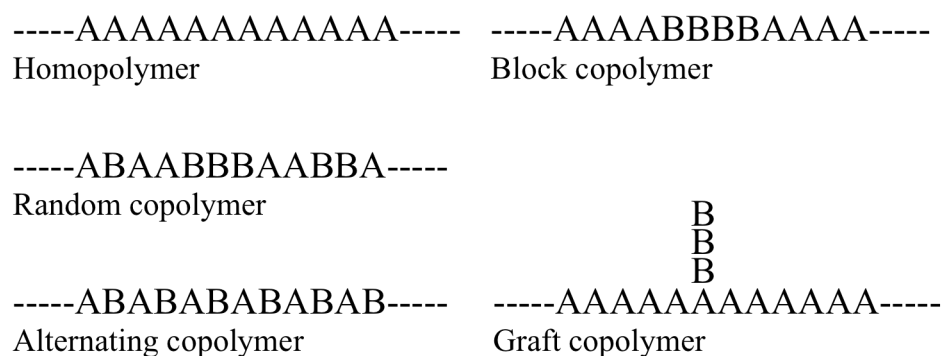


FIGURE 2. Copolymer formulation. Monomer arrangement to give various types of

1.3. POLY(ETHYLENE GLYCOL)

Poly(ethylene glycol) (PEG) is the synthetic polymer of choice in biomaterials and hydrogels due to its hydrophilic nature, coupled with its nontoxic properties and biological compatibility [90, 91]. PEG is synthesized from ethylene oxide and catalyzed in acidic or basic conditions [92, 93]. In Figure 3A, the acid-catalyzed reaction is shown to ring open the epoxide with the help of an anion to yield an ethylene glycol precursor. In the base-catalyzed reaction, the ring-opening step is carried out without the help of an anion or radical, yielding precursors of ethylene glycol. The ethylene glycol produced through the first step can then covalently bond to another ethylene glycol through condensation, eventually yielding a polymer (Figure 3B). The simplicity of the synthesis coupled with the growing role of PEG in biomaterials has led to an increase in the range of molecular weights of PEG that are being manufactured. Likewise the efficiency of synthesis has also given rise to branched, star, and dendrimer PEGs that can be used to covalently attach to biomaterials. Figure 4 shows a sample of the structures in which PEG can be synthesized and used.

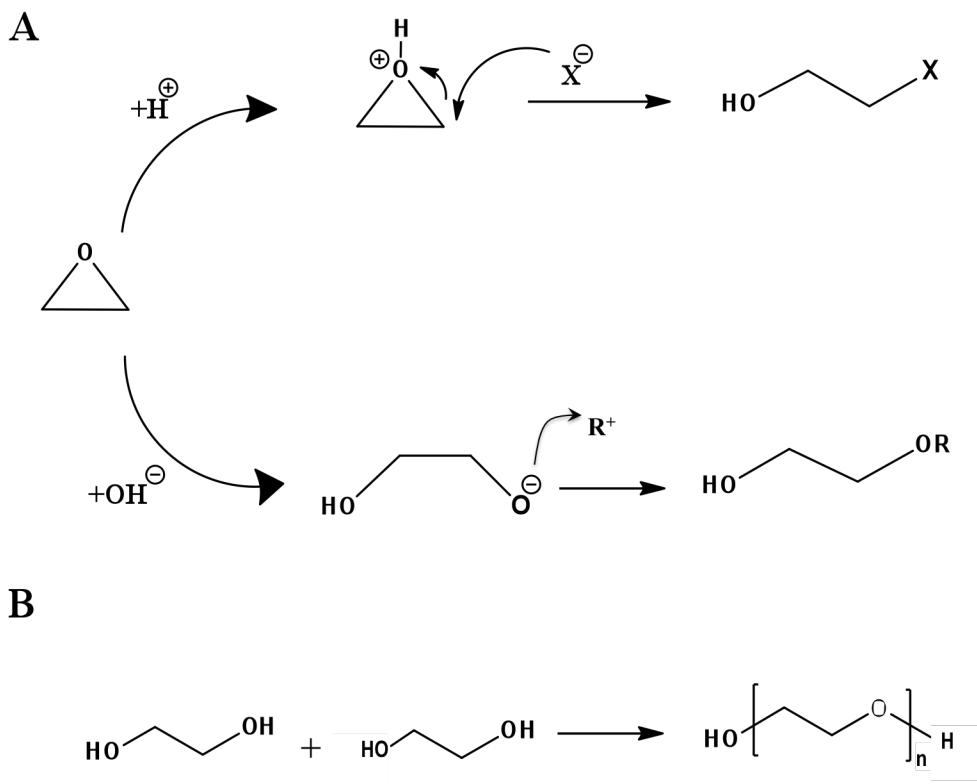


FIGURE 3. Poly(ethylene glycol) synthesis. **A)** Ethylene glycol is synthesized by opening of ethylene oxide in either acidic or basic conditions. **B)** Ethylene glycol is then polymerized into poly(ethylene glycol) via a condensation reaction.

The process of attaching PEG to materials is known as PEGylation and it is used to apply the properties that make PEG biocompatible to materials. Through PEGylation, the biomaterial increases its hydrophilicity and biocompatibility, while decreasing its toxicity and limiting its immunogenicity [94-96]. PEGylation also has the added benefit of preventing the removal of small molecular weight material through the kidneys and increasing the circulation time of drugs and particles in the blood stream by increasing their overall size [94-99]. As illustrated by Figure 5, PEG can be attached to nanoparticles, hydrophobic polymers, carbohydrates and peptides. In the work herein described, four-arm polyethylene glycol will be used as a building block in the formation of the hydrogel, as shown in Figure 1.

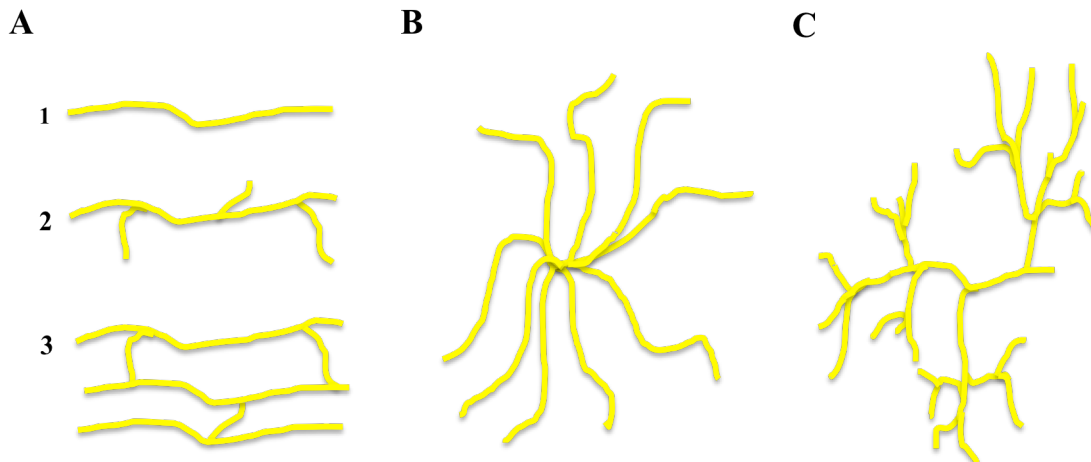


FIGURE 4. Polymer configurations. Forms in which PEG and other polymers can be synthesized and used. **A)** 1A) Linear Polymer, 2A) Branched Polymer, 3A) Network. **B)** Star polymer. **C)** Dendrimer Polymer.

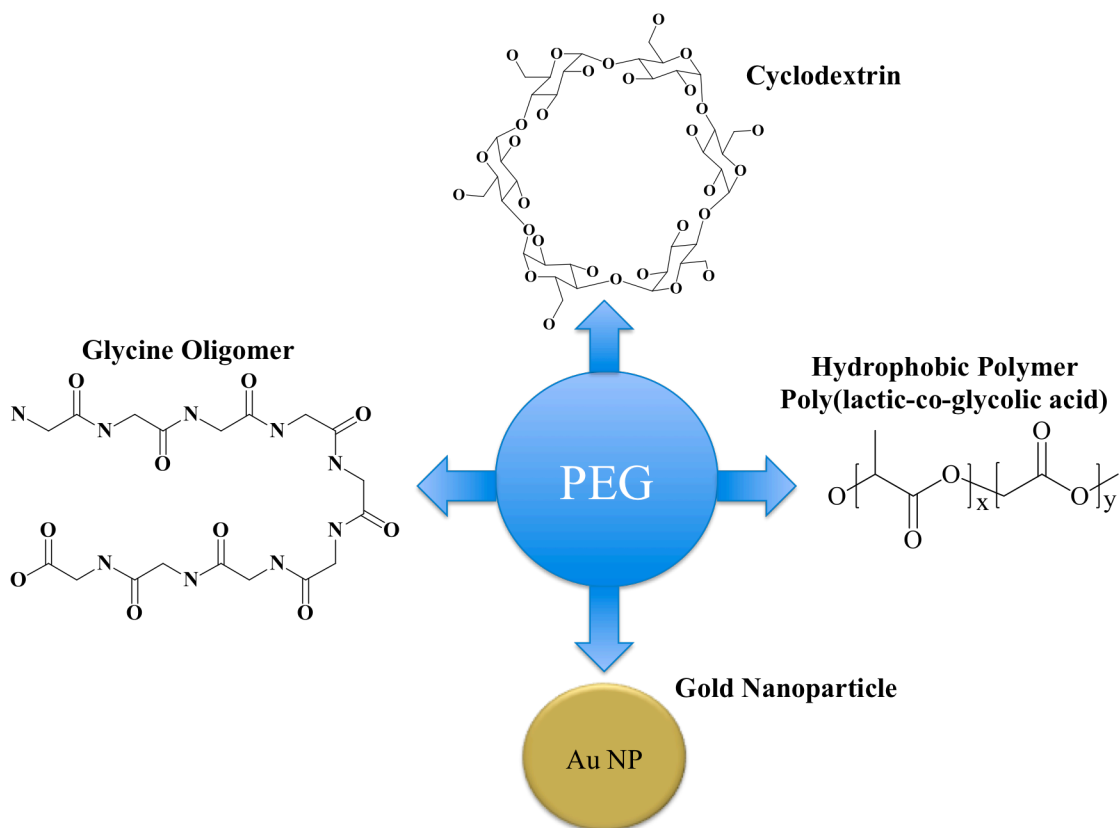


FIGURE 5. PEGylation of various macromolecules. Various macromolecules that are typically PEGylated for biomedical applications as a means of increasing their biocompatibility and stability.

1.4. APTAMERS

First developed by Andrew Ellington, aptamers are high affinity ligands that are formed from nucleic acids [100]. The first aptamers developed utilized double stranded and single stranded RNA (ssRNA) strands, although soon after ssDNA aptamers were described to bind with the same affinity as their RNA counterparts [101-105]. DNA aptamers were specifically sought after because of their added stability both *in vivo* and *in vitro* which provided flexibility of molecular targets. The first single-stranded DNA (ssDNA) aptamer described was a fifteen base oligomer that was specific for the protein thrombin [106]. Interestingly, it was determined that the aptamer formed a specific tertiary structure. This particular aptamer formed a structure that looks like a chair in order to bind efficiently to the thrombin protein [106]. As more and more aptamers were developed, it was shown that indeed most aptamers formed specific tertiary structures and that their binding depended on achieving the tertiary structure [107-109]. Aptamers were determined to depend on physiological conditions to stabilize hydrogen bonding that stabilizes the structure [110-112]. The three-dimensional structure was found to be a result of repulsion forces between the negatively charged backbone and the polymer strand trying to adopt the lowest energy conformation possible [110, 113-115].

Although responsiveness in our hydrogel could be achieved using one of the aforementioned monomers, polymers, or crosslinkers, the aim of this work was to develop a hydrogel that was responsive to a specific molecular stimulus. In order to achieve this level specificity, a DNA aptamer, which has a high affinity for the VEGF protein was chosen. Utilizing a DNA-based aptamer complex avoids nonspecific degradation by hydrolysis of polyester-based biomaterials, or that is caused by proteases

secreted naturally by the cells. Deoxyribonucleases, enzymes that are able to cleave DNA along the phosphate backbone, are not normally secreted into the interstitial fluid by cells. This ensures that nucleases will minimally interact with our matrix and the degradation of the hydrogel is solely caused by the selective interaction of the aptamer and VEGF.

The VEGF aptamer that will be used to form the hydrogel will be part of a three-strand aptamer complex that will act as a crosslinker, as seen in Figure 6. The aptamer complex is used to hold the aptamer (red) and its extension (black) in place via hybridization with complementary strands Q (blue) and F (green), as seen in Figure 6A. The Q and F strands that will be covalently attached to the four-arm PEG at their free ends (3' of left-side strand and 5' end of right-side strand). Degradation will occur in the presence of the molecular target VEGF (represented by stars) as seen in Figure 6B. The cancer cells (here represented by SKOV-3 ovarian cancer cells) entrapped in the hydrogel network will begin secreting the VEGF protein, which the aptamer complex will recognize and bind. Dehybridization of the complementary strands will occur as the aptamer switches its conformation, causing the degradation of the matrix.

The biomolecule target that was chosen in creating the biodegradable scaffold for cell culture is vascular endothelium growth factor (VEGF). VEGF is primarily responsible for promoting angiogenesis as cancer cells grow and proliferate [2, 3, 116-119]. Ovarian cancer cells (SKOV-3) were selected to test the hydrogel as a cell culture platform. This cell line is known to secrete VEGF in large quantities in order to promote vascularization [120]. For this reason this protein makes an important molecular target in the construction of a platform that is intended to be molecularly responsive. In order to target this protein,

an aptamer was chosen that is specific for VEGF. This particular aptamer is composed of 25 DNA bases that has been shown to be highly specific and sensitive towards VEGF [2]. Similar to the thrombin aptamer, the VEGF aptamer has been proposed to acquire a structure shown in Figure 7. The aptamer also relies on hydrogen bonding between its bases in order to yield the specific three-dimensional conformation.

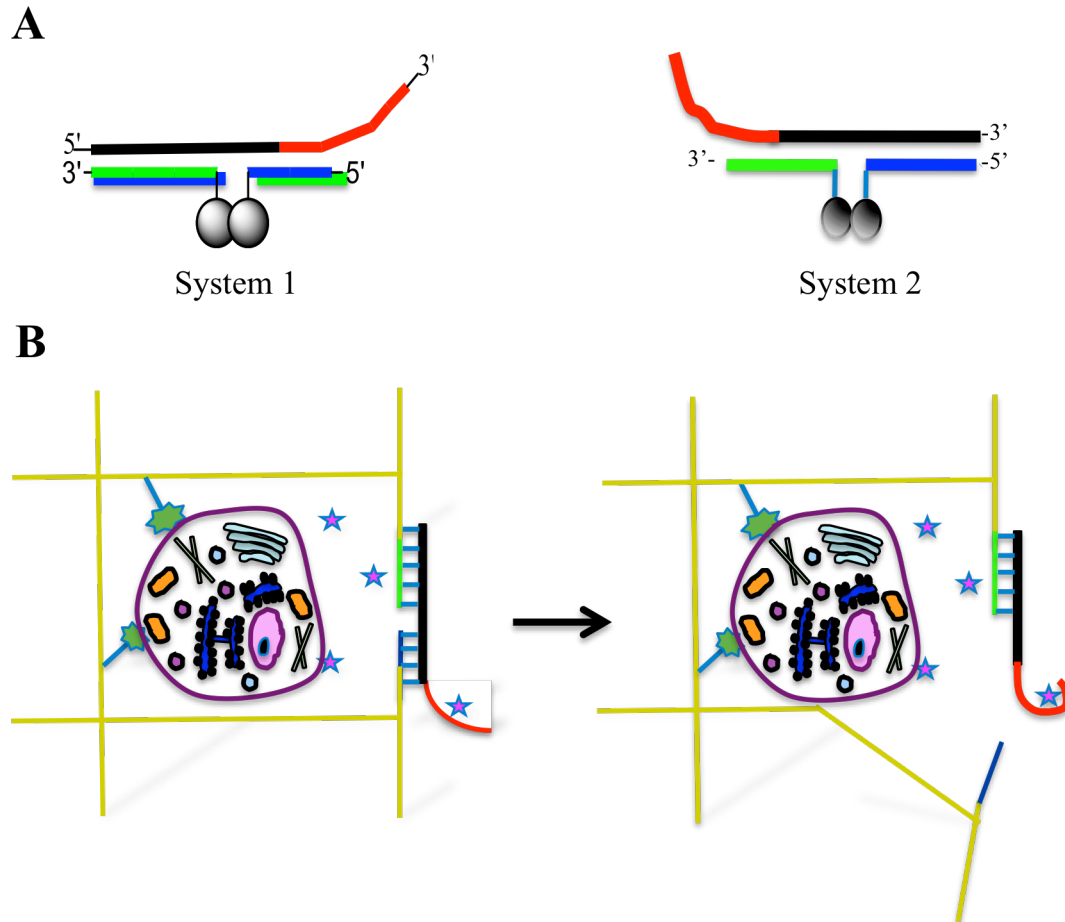


FIGURE 6. Aptamer complex variations and degradation. **A)** Aptamer complex variations studied shown in A. System 1 and 2 are composed of three DNA strands. The aptamer strand consists of the published aptamer sequence (red) extended with a specifically designed oligonucleotide extension (black). In system 1, the 3' end of the aptamer is free, while in system 2 it is the 5' end that is free to interact with the target. **B)** Function of aptamer complex as a molecularly responsive crosslinker that can be disrupted upon interaction with the cell-secreted molecule VEGF (represented by

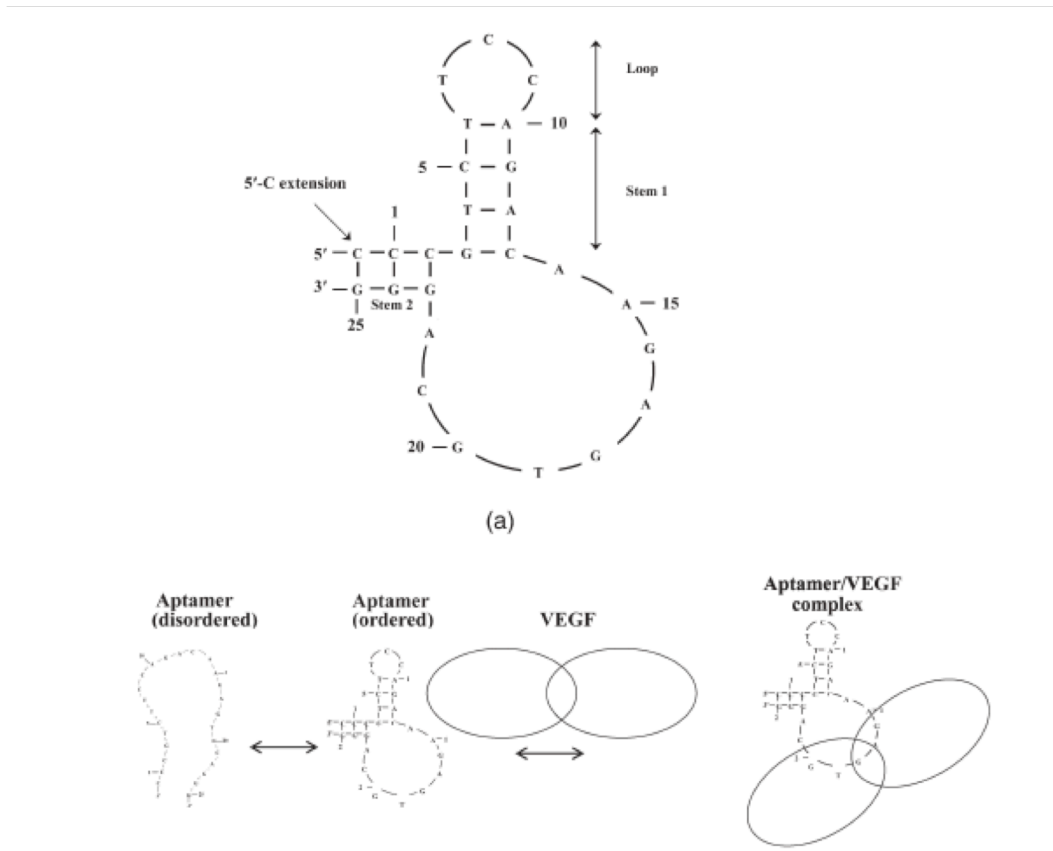


FIGURE 7. VEGF aptamer tertiary structure and VEGF interaction Proposed VEGF aptamer tertiary structure and VEGF interaction [2]

1.5. SYSTEMATIC EVOLUTION OF LIGANDS BY EXPONENTIAL ENRICHMENT

Even though most aptamers range from 17-25 nucleotides, they are able to bind both large and small molecules including, for example, VEGF or cocaine [2, 121-124]. No matter the size of the target, the main objective of the aptamers is to bind with high specificity and efficiency in the presence of the large amount of proteins and biomolecules that are found in and around the cell's environment [125-127]. For this reason, a well-understood method of selecting the ligands with the highest selectivity and affinity has been developed and described [128, 129]. This method is known as

systematic evolution of ligands by exponential enrichment (SELEX) [128, 129]. It involves six primary steps that utilize a large random library of ssDNA or RNA strands introduced to a selected molecular target, as shown in Figure 8. After allowing the oligonucleotides to bind to the target, the remaining strands, which were not specific or are weakly bound to the molecule are then washed off. The oligonucleotide-bound target molecule is then subjected to a detergent or change in pH to denature and separate the oligonucleotides from the target. These oligonucleotide strands are then amplified many

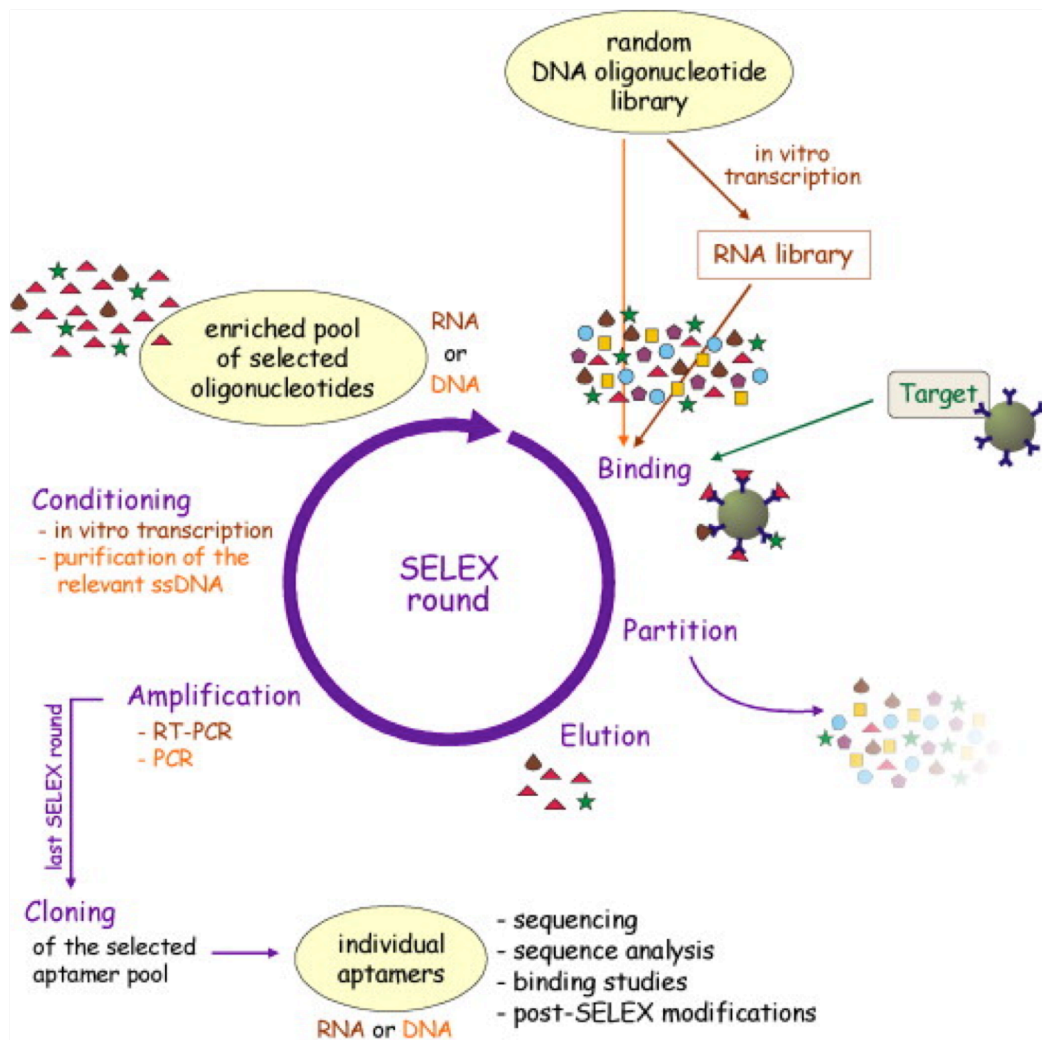


FIGURE 8. Schematic of SELEX process [1].

times and reintroduced to the target molecule once more. The strands with the highest affinity will displace the lower affinity ligands, which are then washed off once more. Again, the bound strands are denatured and removed from the molecule and then amplified. Several cycles (6-20) are conducted until only a few strands remain that can then be characterized by sequencing and their affinity quantified via binding studies. What is produced after these cycles is a highly selective aptamer that can be used in various formats from biosensors and drug delivery systems, to crosslinkers as in this work [130]. Figure 8 illustrates the process starting from a large library of oligonucleotides to quantifying the binding affinity of aptamer.

1.6. VASCULAR ENDOTHELIAL GROWTH FACTOR

In mature organisms endothelial cells secrete vascular endothelium growth factor protein to signal that there is a need for oxygen and nutrients to a particular region. As cancer cells begin to grow and proliferate, the area around them becomes hypoxic due to a large number of cells occupying and vying for limited amounts of oxygen and nutrients. The VEGF protein is then secreted in large quantities to initiate angiogenesis and vascularization [3, 116-119].

VEGF is a homodimer protein that consists of two 19k Da domains covalently linked via disulfide bonds to yield a 38k Da biologically active protein (Figure 9). However, before being secreted from cells, the protein undergoes glycosylation in the golgi apparatus to yield a protein with a molecular weight that ranges from 45-50k Da [131, 132]. The primary form of VEGF has been labeled VEGF₁₆₅ in order to distinguish it from the family of VEGF's that have been identified in humans and other animals [116,

119]. When cells become cancerous and proliferate uncontrollably, they secrete large quantities of VEGF in order to stimulate angiogenesis in the tumor site. This has led to VEGF being established as the primary molecule that induces angiogenesis and has been widely studied and characterized in cancer research. The fact that VEGF is so well understood makes VEGF an ideal molecular target to provide the degradability in our scaffold.

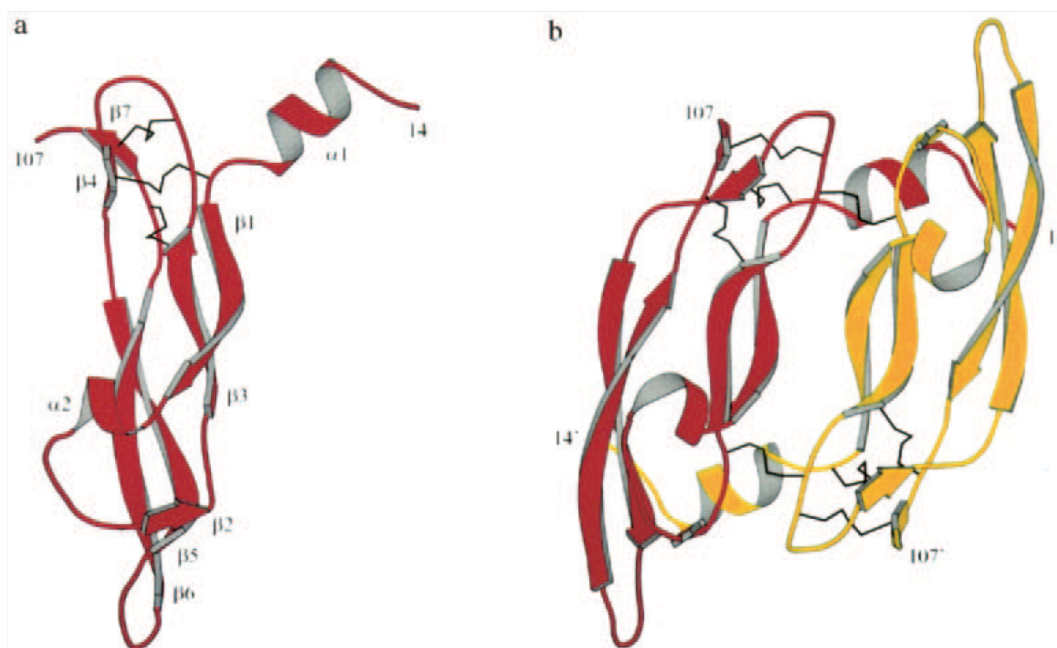


FIGURE 9. VEGF protein. **A)** Structure of one of the proteins that makes up the homodimer. **B)** VEGF protein were the homodimer is linked by disulfide bonds [3].

1.7. COPPER-FREE CLICK CHEMISTRY

Initially, click chemistry encompassed the reaction between an alkyne and azide. Under this umbrella, two different reaction methods have been developed which are known as copper-catalyzed or copper-free click chemistry. Although the reactions yield the same (3+2) cycloaddition, the method in which they do so differs considerably. The

concept of the azide-alkyne reaction was first described in 1963 by the German chemist Huisgen at the University of Munich [133]. The reaction described by Huisgen involved 12-18 hours of reaction time with temperatures of 500 K that produced isomers that were difficult to separate. Due to these limitations, the click chemistry reaction was almost entirely forgotten.

It was not until 2001 when Karl Sharpless described the copper-catalyzed reaction that the world took note of click chemistry once again [134]. Copper-catalyzed click chemistry revolutionized the way in which biomolecules were functionalized and manipulated by providing a sensitive reaction method that covalently “clicked” a primary alkyne with an azide. [133, 135, 136]. What really stood out about the reaction described by Sharpless is that the reaction could be conducted through a wide pH and temperature

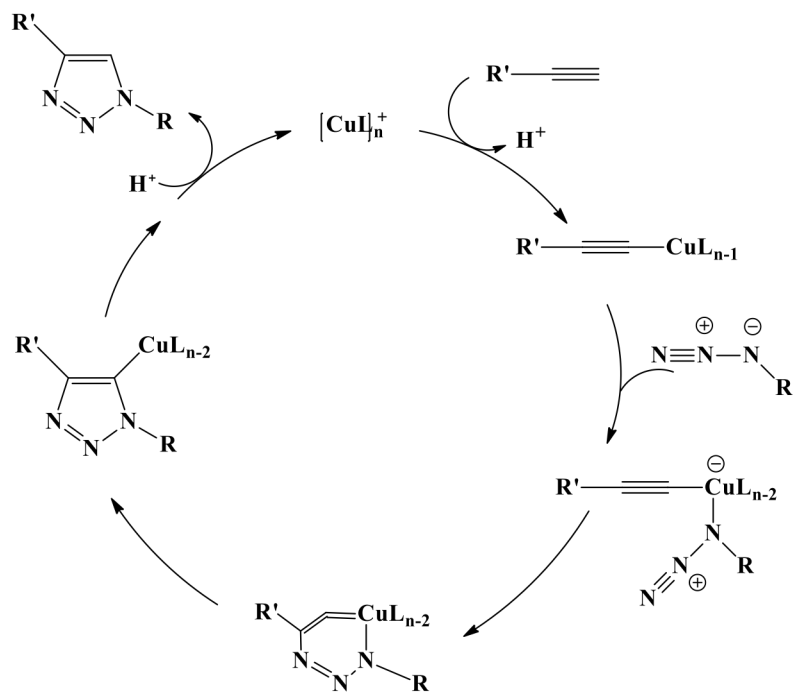


FIGURE 10. Schematic of copper-catalyzed click chemistry reaction. Copper-catalyzed click chemistry reaction. Copper (I) coordinates electron exchange between azide and terminal alkyne [4].

range. The active Cu(I) is able to coordinate the electron exchange between the alkyne and the azide effectively as seen in Figure 10, thus yielding a cycloaddition in minimal time compared to the uncatalyzed reaction with high yield and rates. Researchers favored the reaction because it allowed effective modification of biomolecules with limited interaction between the azide and alkyne groups with biological processes. However, carrying out this reaction in biological systems proved toxic due to the use of the copper catalyst that negatively affects cells and interferes with biological processes [137-139].

Carolyn Bertozzi first described copper-free click chemistry in 2007 as a means to expand the role of click chemistry reactions into living organisms [140]. Through the use of highly strained cyclooctyne it was found that the click reaction occurred in the absence of the copper catalyst. It was also shown that the highly strained cyclooctyne allowed the reaction to occur faster and with higher yields compared to the Copper (Cu)-catalyzed reaction. It is postulated that upon contact between the azide and alkyne group, the transfer of electrons occurs rapidly, as shown in Figure 11. The reaction not only performed better than the Cu-catalyzed reaction but was also deemed 100% bioorthogonal. Due to its biocompatibility with organisms, Cu-free click chemistry has

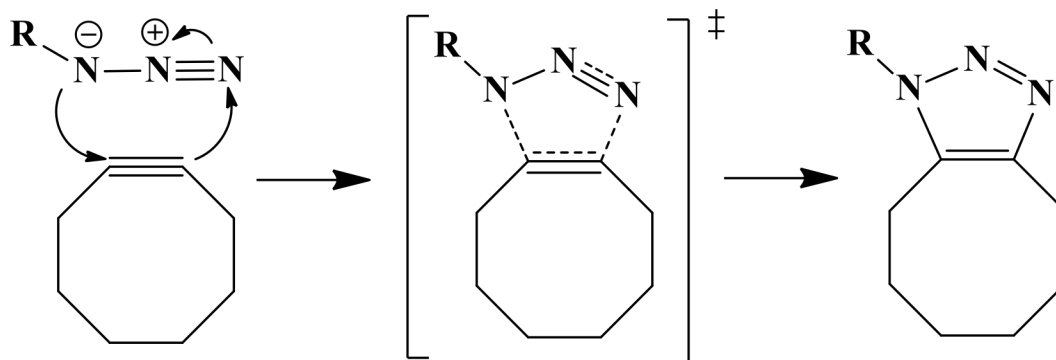


FIGURE 11. Schematic of copper-free click chemistry reaction. (3 + 2) addition of azide to cyclooctyne.

been used to modify biomolecules as well as to carry out conjugation reactions *in vitro* and *in vivo*. The hydrogel that is being synthesized in this work will utilize copper-free click chemistry to anneal the DBCO functionalized 4-arm poly(ethylene glycol) polymer to the azide-functionalized aptamer complex, as shown in Figure 1. By utilizing Cu-free click chemistry, the synthesis of the matrix could be carried out at biological temperature in a one-pot synthesis in order to enable the encapsulation of cancer cells within the matrix.

2. DESIGN AND EVALUATION OF APTAMER COMPLEX

As mentioned in Chapter 1, the overall objective of this work is to develop hydrogels that can respond to molecular stimuli and that could be prepared under mild conditions to enable the incorporation of live cells within them. To do this, we sought to incorporate aptamer complexes as crosslinkers of four-arm polymer strands. The three-part aptamer complex shown in Figures 1 and 6 was designed to enable the mostly free aptamer to interact with a target and, in the process, change its conformation and competitively displace a partially complementary strand, thus disrupting the hydrogel crosslink.

In order to properly design the aptamer complex, it was important to account for and properly utilize the ability of deoxyribonucleic acids to form complementary base pairs (guanine to cytosine, and adenine to thymine) with each other via hydrogen bonding [141, 142]. Although the hydrogen bond is considered a weak bond (7-10 kJ), the cumulative strength of the number of hydrogen bonds in a DNA polymer complex has the ability to anneal the strands strongly together [143-146]. However, being that a single hydrogen bond is easily broken in DNA, at any given time there are hydrogen bonds being broken and formed. In order to quantify the cumulative strength that the hydrogen bonds have over the length of DNA strand a method to determine the melting temperature (T_m) of the hybridized oligonucleotide complex has been developed [147]. The melting temperature measures the strength of the oligonucleotide hybridization and specifies a temperature at which the oligonucleotide strands will have 50% of the nucleotides paired with their complementary base and 50% dissociated. However, the length of the

oligonucleotide is not the only determining factor when calculating T_m . A major source that contributes to the overall T_m is the presence of monovalent (Na^+ and K^+) and divalent salts (Mg^{2+} or Ca^{2+}) that help to stabilize the DNA-to-DNA interactions [148, 149].

Scientists at Integrated DNA Technologies (IDT) have developed models for the prediction of DNA hybridization under a range of biochemical conditions. The free software OligoAnalyzer 3.1 developed from these models can be used to estimate the T_m of an oligonucleotide [150-153]. The algorithm is able to account for both monovalent and divalent salt concentrations as well as DNA concentration to predict the T_m . Equations 1 and 2 describe the functions developed by IDT to provide corrections for salt dependency of the T_m [150-155].

Equation 1: Sodium dependent equation.

$$\frac{1}{T_m(\text{Na}^+)} = \frac{1}{T_m(1\text{ M Na}^+)} + \{(4.29f_{GC} - 3.95) \ln[\text{Na}^+] + 0.940 (\ln[\text{Na}^+])^2\}$$

Equation 2: Magnesium dependent equation.

$$\begin{aligned} \frac{1}{T_m(\text{Mg}^{2+})} = & \frac{1}{T_m(1\text{ M Na}^+)} + a + b \ln[\text{Mg}^{2+}] + f_{GC} \times (c + d \ln[\text{Mg}^{2+}]) \\ & + \frac{1}{2(N_{bp} - 1)} \times [e + f \ln[\text{Mg}^{2+}] + g (\ln[\text{Mg}^{2+}])^2] \end{aligned}$$

were:

$T_m(\text{Na}^+)$	=	T_m at a given Na^+ molarity
$T_m(\text{Ca}^{2+})$	=	T_m at a given Ca^{2+} molarity
$T_m(1\text{ M Na}^+)$	=	T_m at a 1 M Na^+
f_{GC}	=	Fraction of G and C nucleotides in sequence
$[\text{Na}^+]$	=	Na^+ molarity
$[\text{Ca}^{2+}]$	=	Ca^{2+} molarity

The parameters “a” through “g” of equation 2 are as given in Table 1.

TABLE 1. Fit parameters for equation 2

Parameter	Value [K⁻¹]	Standard Error [K⁻¹]
<i>a</i>	3.92 x 10 ⁻⁵	0.2 x 10 ⁻⁵
<i>b</i>	-9.11 x 10 ⁻⁶	0.5 x 10 ⁻⁶
<i>c</i>	6.26 x 10 ⁻⁵	0.4 x 10 ⁻⁵
<i>d</i>	1.42 x 10 ⁻⁵	0.08 x 10 ⁻⁵
<i>e</i>	-4.82 x 10 ⁻⁴	0.7 x 10 ⁻⁴
<i>f</i>	5.25 x 10 ⁻⁴	0.2 x 10 ⁻⁴
<i>g</i>	8.31 x 10 ⁻⁵	0.2 x 10 ⁻⁵

The OligoAnalyzer program was used to design the aptamer complex that was used to crosslink the molecularly responsive hydrogels. Key parameters that needed to be considered in the design of the aptamer crosslinks included the restricted nucleotide sequence of the aptamer itself, the need for the three-part aptamer complex to be stable at room and physiological temperature (37 °C), and the need for the aptamer to be able to interact with the target and, in the process, dehybridize from at least one of the partially complementary strands.

2.1. MELTING TEMPERATURE SIMULATION FOR DNA COMPLEX

Simulations of the proposed aptamer complex were conducted to determine the proper oligonucleotide sequences that would provide optimum melting temperatures for the aptamer complexes. Two conformations of the aptamer complex were proposed, as shown in Figure 6. Three aims needed to be met by the proposed aptamer complex in order for it to be considered as a viable option for acting as a crosslinker. Aim one is that

the design of the aptamer complex must not include palindromes or sequences that would cause the aptamer complex strands to anneal to themselves or in a fashion that was unwanted. The aptamer strands F and Q must preferentially hybridize with the extended aptamer strand at the designated location (Figure 12). They should not compete with one another for a binding region or themselves interact with other molecules secreted by the cell. Aim two is that the proposed conformations would allow the complementary strands (F and Q) to anneal to the elongated aptamer strand (L) with enough affinity and fidelity to form a strong crosslink and, in the process, quench the fluorescence molecule F with the quencher Q to enable monitoring of the complexation status. Aim three is that the complementary strands would anneal at varying affinities and strength. The role of the varying affinities would be used to cause the dissociation of the complementary strand nearest to the aptamer (strand Q in System 1 and strand F in System 2) as the aptamer binds to the molecular target, thus providing a molecularly controlled degradable crosslinker for the hydrogel.

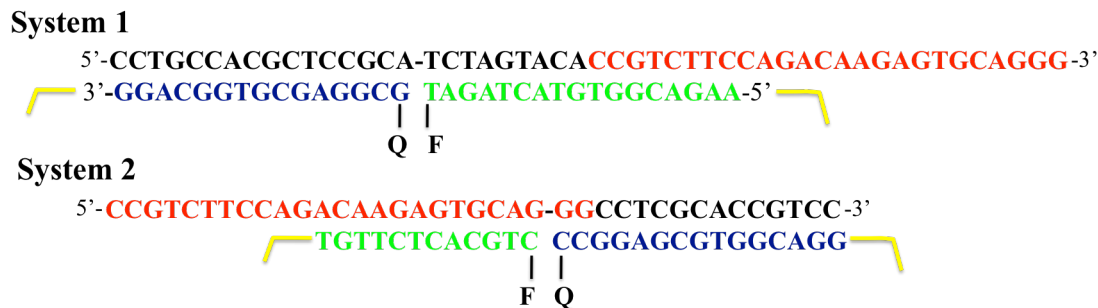


FIGURE 12. Design of aptamer complex. Two variations of the aptamer complex were developed using three complementary DNA strands (System 1 and System 2). Strand L contains the aptamer (red strand) and extension (black strand). Strand F is the green-labeled DNA strand and contains 6-carboxyfluorescein (F). Strand Q is the blue-labeled strand and contains proprietary Black Hole Quencher 1 (Q).

The hybridization affinity of strand F and Q to strand L and stability of the complex were indirectly assessed through the determination of melting temperature of the complexes. The use of T_m allowed us to confirm that the complex would remain hybridized at 37 °C but dissociate easily above this temperature. The ideal temperature for the strand that is meant to dissociate (the strand that is hybridized to the aptamer, i.e. the Q strand in System 1 and the F strand in System 2), was postulated to be 45 °C (high enough above physiological temperature to remain complexed in this state but low enough to enable dehybridization upon interaction of the aptamer with the target). Since the remaining strand (that one which is hybridized to the black aptamer extension, i.e. the F strand in system A and the Q strand in system B) is meant to remain hybridized, a T_m of approximately 60 °C was targeted for this strand.

2.1.1. MATERIALS AND METHODS

IDT OligoAnalyzer 3.1 was used to determine T_m of hybridization between strand F and Q of System 1 and 2 and their respective complementary strands. The binding affinity was determined by varying monovalent and divalent salt concentrations in order to simulate physiological conditions. Table 2 list the variables used to determine T_m .

TABLE 2. Monovalent and divalent concentrations used to determine T_m

[NaCl] mM	[Mg ²⁺] mM
5	0.4
25	0.6
50	0.8
75	1.0
100	1.2
125	1.4
150	1.6
175	1.8
200	2.0
225	
250	

The ECM salt concentration in mammalian cells is 150 mM NaCl and 0.8 mM Mg²⁺ [5].

2.1.2. RESULTS AND DISCUSSIONS

The aptamer complex was designed taking into account the specific nucleotide sequence of the aptamer, which could not be modified. The sequence of the aptamer extension and the two complementary strands F and Q had to be selected and adjusted (by increasing or decreasing the overall number of nucleotides, G/C content, of number of base pairs hybridized with the L strand) in order to obtain the desired complex properties. This selection and adjustment process was aided by the OligoAnalyzer software, which provides an indication of the melting temperature and binding affinity of oligonucleotides. Results are shown here for the two final systems that were selected and further used in experimental protocols.

The oligomer strands Q (5-GCGGAGCGTGGCAGG-3) and strand F (5-AAGACGGTATACTATT-3) from System 1 were entered into the IDT OligoAnalyzer

program at the salt concentrations listed in Table 2. The resulting melting temperatures were plotted in a three dimensional graph in order to compare both mono and divalent salts to the melting temperature. Figure 13 represents the results of the calculated melting temperature for both strand Q (Figure 13.A) and strand F (Figure 13.B).

The aim of strand F in System 1 is to anneal to the black extension of the L strand (5'-CCTGCCACGCTCCGCATCTAGTACACCGTCTTCCAGACAAGAGTGCAGGG-3') strongly enough that it would remain hybridized after the aptamer interacts with the target molecule. For this reason, a T_m in the range of 60-70 °C was desired. To satisfy the need for the strong binding interaction with the least amount of nucleotides, an oligomer with high G and C content was developed. Figure 13A indicates that the melting temperature of strand F with its complement at physiological conditions (150 mM NaCl and 0.8 MgCl₂) will be 64 °C.

Furthermore the hybridization of strand Q to the L strand was shown to be strong enough (stable at physiological temperature) at the lower end of the salt concentration, resulting in a T_m 58 °C at 5 mM NaCl and 0.4 mM MgCl₂. At the highest salt concentration tested, 250 mM NaCl and 2.0 MgCl₂, the hybridization T_m plateaus at 66 °C.

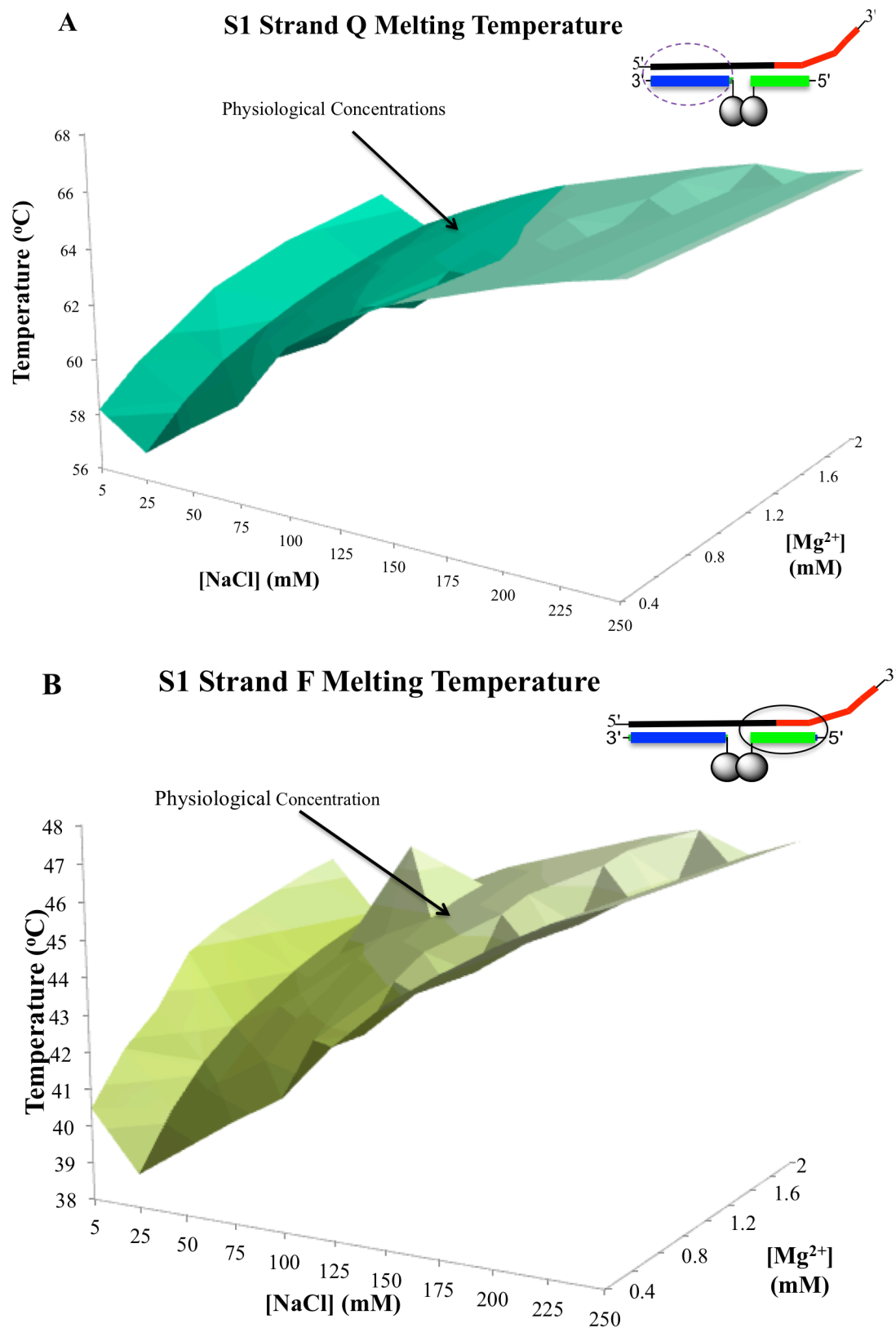


FIGURE 13. Melting temperature of (A) strand Q and (B) F of System 1 (S1).

Strand F of System 1 is meant to dissociate as the aptamer interacts with the target molecule. The aim is to create an oligomer with a T_m range of 40-50 °C. The selected sequence consists of a sixteen-nucleotide oligomer that is estimated to hybridize with a T_m of 44 °C at physiological salt concentrations (Figure 13B). The oligomer was estimated to have a T_m of 40 °C at 5 mM NaCl and 0.4 mM MgCl₂ and at T_m of 47 °C at 250 mM NaCl and 2 mM MgCl₂ (Figure 13B). The results indicate that the complex will remain hybridized at physiological temperature (37 °C) but bind weakly enough to allow the strand to dissociate from its hybrid (aptamer and part of the extension) upon aptamer interaction with the VEGF target.

System 2 is based of the same concept as System 1 were strand F (5-CTG CACTCTTGT-3) and Q (5-GGACGGTGCGAGGCC-3) have varying binding affinities to their specific binding regions of the linker (L) strand. The difference between the complex is the inversion of the aptamer on the linker strand (5-CCGTCTTCCAGACAAGAGTGCAGGGCCTCGCACCGTCC-3). In System 1 the aptamer is found on the 3' end of the linker (L) strand; however, on System 2 the aptamer is located on the 5' end, as shown in Figure 12. The selected strands F and Q of System 2 were tested on the IDT OligoAnalyzer 3.1 program to determine the hypothetical melting temperature.

Strand Q of System 2, which is meant to remain hybridized to the linker strand, was designed as a 15-nucleotide oligomer with high G and C ratio. The strand was estimated to have a melting temperature of 66 °C at physiological conditions, as shown in Figure 14A. The T_m range of hybridization for strand Q ranged from 60.5 °C at 5 mM NaCl/0.4 mM MgCl₂ to 68.4 °C at 250 mM NaCl/ 2.0 MgCl₂. Based on the T_m range, it is

hypothesized that Strand Q has a high enough binding affinity to remain annealed to the linker strand even after the aptamer interacts with the molecular target.

Strand F of System 2, which binds to the aptamer, was designed to be the weaker binding of the two. It comprises a twelve-nucleotide oligomer with an estimated T_m of 44 °C at physiological salt conditions. The T_m of strand F to its complement was shown to range from 40 °C at 5 mM NaCl/0.4 mM MgCl₂ 48 °C at 250 mM NaCl/2.0 mM MgCl₂, as shown in Figure 14B. Based on the T_m range of strand F, it is hypothesized that this strand will be able to remain hybridized at 37 °C but dissociate from the linker strand as the aptamer interacts with the target molecule.

The IDT OligoAnalyzer program is meant to provide a reference of the theoretical melting temperature for an oligomer based on the parameters of Equation 1. As can be seen from the graphs produced both on Figures 13 and 14, the contour maps do not represent a true linear relationship but, instead, deviate to produce dips and valleys suggesting that the equation is unable to account accurately for all the variables. Noticeably the program is also unable to account for salt concentrations beyond 250 mM NaCl and 2.0 mM MgCl₂. At concentrations higher than these, the graph plateaus and produces no change in melting temperature. This could be attributed to either the negatively charged phosphate backbone being completely saturated with positive monovalent or divalent ions produced from the solvation of the NaCl and MgCl₂. At this point, additional cation content becomes negligible in the DNA hybridization. However, the use of the program allows us to utilize the overall trend as a reference to determine a preliminary starting point. Through the use of the program, the two aptamer systems utilized were developed with a T_m that would allow dissociation.

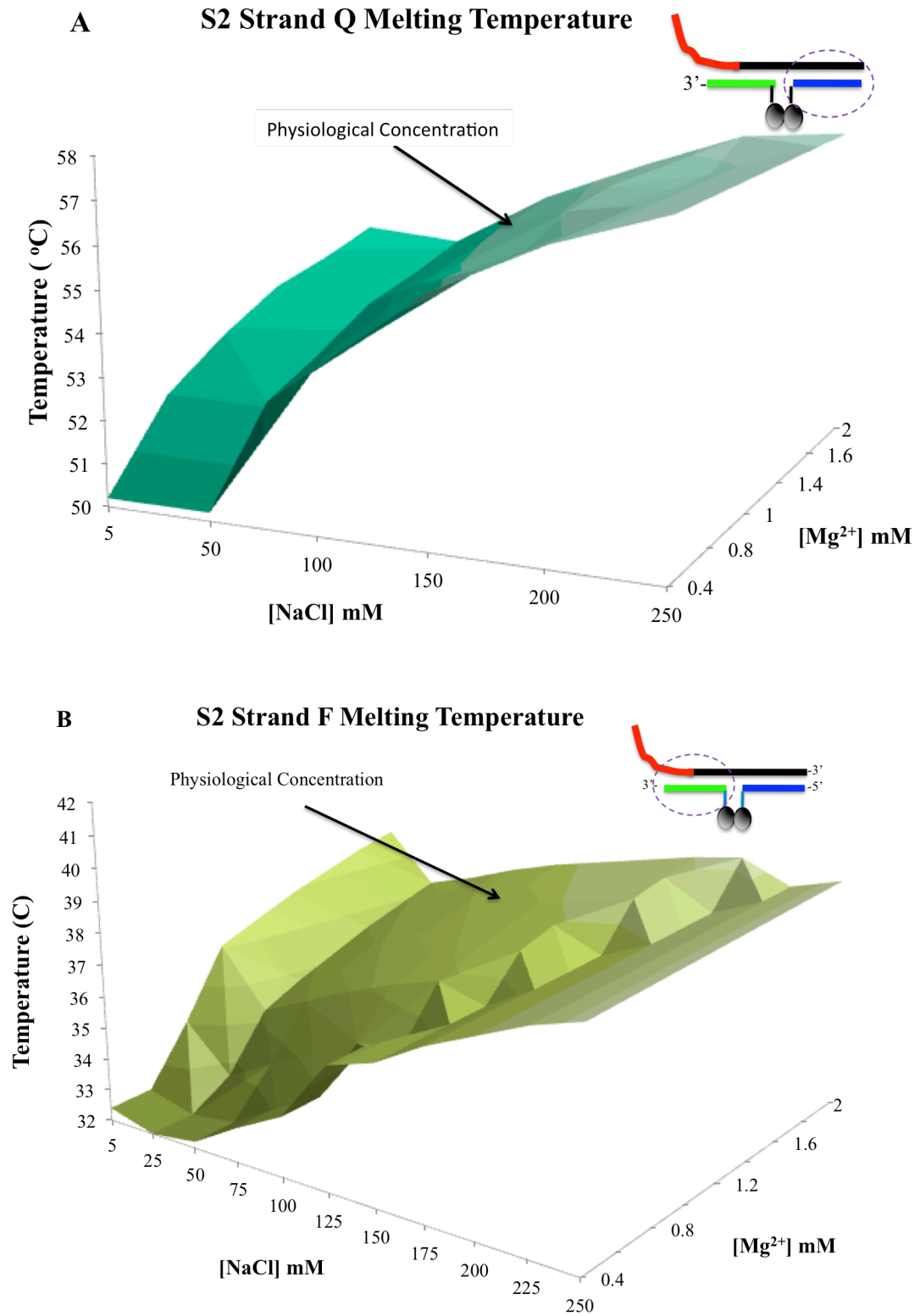


FIGURE 14. Melting temperature of (A) strand Q and (B) F of System 2 (S2).

2.2. MONITORING OF SYSTEM 1 AND SYSTEM 2 COMPLEX FORMATION VIA FLUORESCENCE

F strands on both systems were covalently labeled with 6-fluorescein amidite (6-FAM) which is a common fluorescent dye used in labeling DNA due to its water solubility properties and absorbance (492 to 517 nm) outside the range in which DNA absorbs (260 nm), as shown in Figure 12 A and B. Strands Q of each system were functionalized with IDT's proprietary black hole quencher 1 (BHQ1). This particular quencher is able to absorb light in the 400-650 nm range with no native emission. Together the fluorophore and quencher will be used for Förster resonance energy transfer (FRET) to signal that the complex has formed as hypothesized. Since both molecules will be located adjacent to one another when the complex is formed, the energy released by the fluorophore will be completely absorbed by the quencher [156-158]. As long as the molecules remain within 1-10 nm, as expected when the complex has hybridized, there will be quenching observed. On the other hand, when the aptamer complex is disrupted either by interaction with the target or temperature-induced melting, fluorescence will be observed. In order to verify the binding affinity of the proposed complex, FRET was used to monitor complex formation and disruption.

2.2.1. MATERIALS AND METHODS

The following DNA strands that make up the complexes of System 1 and 2 were purchased from Integrated DNA Technologies (Coralville, IA) with the indicated modifications:

System 1

Linker: 5'-CCTGCCACGCTCCGCATCTAGTACACCGTCTTCCAGA

CAAGA GTGCAGGG-3' (VEGF aptamer is underlined)

F Strand: 5'-TAGATCATGTGGCAGAA-6-FAM-3'

Q Strand: 5'-BHQ1-GGACGGTGCGAGGCG-3'

System 2

Linker: 5'-CCGTCTTCCAGACAAGAGTGCAGGGCCTCGCACCGTCC-3'

(aptamer is underlined)

Q Strand: 5'-CCGGAGCGTGGCAGG-BHQ-1-3'

F Strand: 5'-6FAM-TGTTCTC ACGTC -3'

The DNA strands of System 1 and 2 (L, Q, and F) were each placed in a buffer containing 10 mM of Tris(hydroxymethyl)aminomethane (TRIS) (Thermoscientific) at a concentration of 100 μ M at pH 7.4. Concentrations were calculated using optical density (OD) at a wavelength of 260 nm using a microplate reader (Biotek Synergy H4 Multi-Mode Plate Reader). DNA strands were combined at a 1:1:1.5 molar ratio of F:Q:L. The strands were combined at ten times the desired final concentration and combined by placing 11 μ L of each strand into an 1.5 mL microcentrifuge tube. The DNA was then diluted by adding 77 μ L of buffer to a final volume of 110 μ L. The buffers were used to dilute such that the final salt concentrations were as shown in Table 3. The DNA was then heated and shaken to 95 °C in a thermomixer (Eppendorf 5425 microcentrifuge). The temperature was maintained for 5 min and then allowed to cool to 25 °C. The DNA was then centrifuged (Eppendorf) at 1250 x g for 2 min to collect the condensed volume

and allowed to rest for 3-4 hours. Controls containing strand F and Q strands only at concentration 1:1 of F:Q were prepared by adding 11 μL of each strand at 10x concentration and diluting with buffer to 110 μL . A second control containing only strand F was placed at 10-fold the desired concentration by adding 11 μL and diluting to 110 μL . The controls were then subjected to heating, centrifugation, and resting time exactly as for the three-strand complexes above. Aptamer complexes and controls were added to 5 wells each of a 384 well plate at a volume of 20 μL per well. Complex formation was monitored via fluorescence using the Biotek plate reader. Readings were taken every 5 minutes for 45 minutes.

TABLE 3. Buffer concentrations used in quenching study for Systems 1 and 2

System 1			System 2
Trial 1	Trial 2	Trial 3	Trial 4
[NaCl] mM*	[NaCl] mM, 1 mM CaCl_2 *	[NaCl] mM, 1 mM MgCl_2 *	[NaCl] mM, 1 mM MgCl_2 *
0	0	0	0
25	25	25	10
50	50	50	25
			50
			75
			100

Note: buffers included 10 mM Tris at pH 7.4. NaCl (BDH) and MgCl_2 (Sigma Aldrich).

2.2.2. RESULTS AND DISCUSSIONS

The resulting data for the quenching study from trials 1-3 (System 1) was plotted on Figure 15 and that of trial 4 (System 2) was plotted on Figure 16. The first three trials utilized System 1 to determine the optimal divalent and monovalent salt concentration that would enable proper formation of the complex, as confirmed by fluorescence

quenching. The fluorescence data was corrected by subtracting the fluorescence given by a buffer control, and then normalized by dividing the corrected fluorescence of each strand by the fluorescence of the control containing strand F alone. This method ensures that strand F is the maximum fluorescence that could be produced.

Trial 1 utilized no divalent ions in the buffer. The resulting data was plotted on Figure 15A. Results showed that the complex formed with zero Na^+ ions quenched the most, with 0.41 normalized fluorescence (NF). At concentrations of 25 mM and 50 mM NaCl, the NF measured 0.50. Results of trial 2 in which complex formation occurred in a solution containing 1 mM of CaCl_2 , are plotted on Figure 15B. The complex formed in 0 mM NaCl produced 0.44 NF, while that in 25 mM and 50 mM NaCl showed 0.48 and 0.50 NF, respectively. Finally, trial 3 utilized 1 mM of Mg^{2+} divalent ions. The resulting graph, Figure 15C, shows that the complex formed in 0 mM NaCl produced a NF of 0.41, while in 25 mM NaCl it produced a NF of 0.48, and in 50 mM NaCl a NF of 0.50.

The aptamer complex used for trial 1-3 (System 1) showed relatively poor quenching, having suppressed the fluorescence of Strand F alone by only approximate 2.5-fold. Standard deviations suggest that there is a statistically significant difference in the extent of quenching of the complexes formed at 0 mM NaCl from those the other two NaCl concentrations in all three trials.

Interestingly, the control, which contained only the strand F and Q had a higher NF than Strand F by itself. This could be caused by possible intermolecular interactions and quenching between F strands on the F-only sample, in comparison to more extensive repulsion forces between the F and Q DNA strands in the second control were the overall DNA strand concentration is higher. At these low monovalent and divalent ion

concentrations it is possible that the repulsive forces are stronger than the hydrogen bonds that could be formed between strand Q and F. Separate studies at higher (above physiological) NaCl concentration showed that at this higher Na⁺ concentration the NF of the control containing both F and Q strands was lower than that of the control containing only the F strand (data not shown). This suggests that at the higher salt concentrations, repulsions are minimized due to cation-induced stabilization of the oligonucleotides. Further studies will need to investigate this hypothesis.

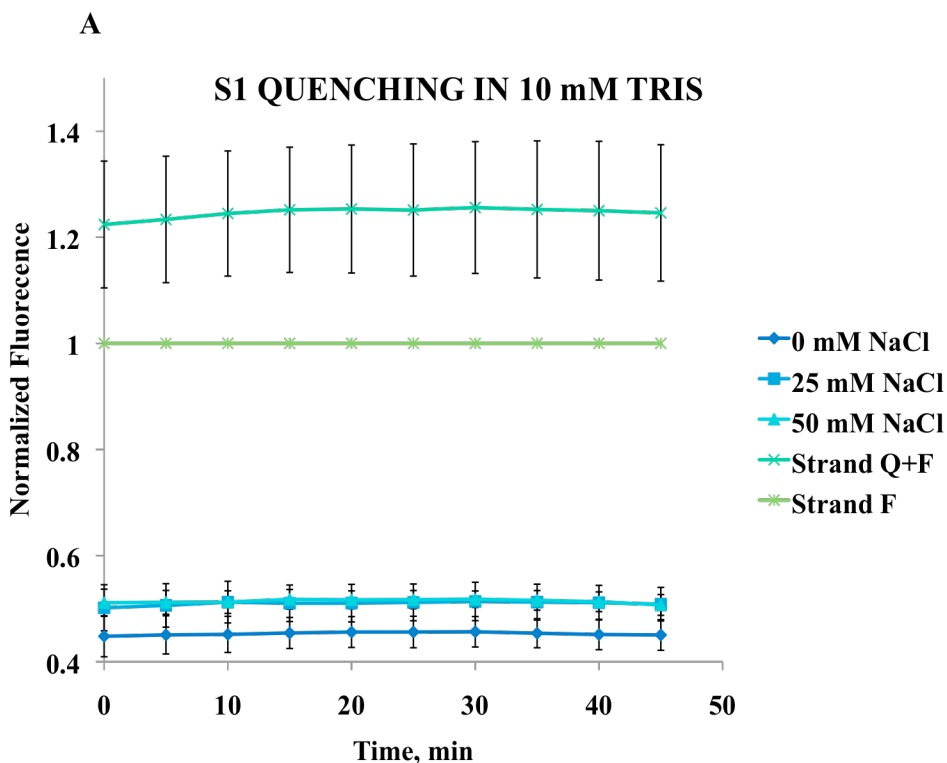


FIGURE 15. Quenching of System 1 (S1) at various NaCl concentration. **A)** Trial 1 used zero divalent ions. **B)** Trial 2 Utilized 1 mM of CaCl₂. **C)** Trial 3 utilized 1 mM of MgCl₂. Each data point is an average of 5 readings. Error bars indicate the standard deviation.

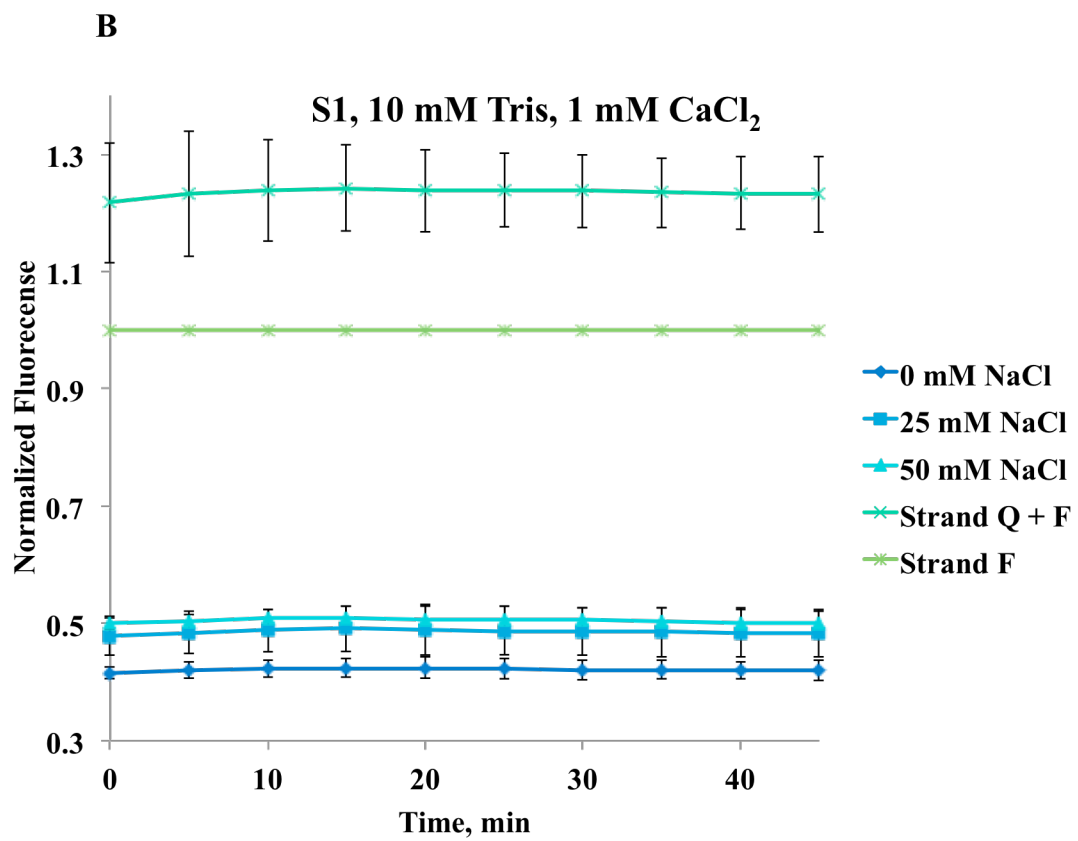


FIGURE 15. Continued.

C.

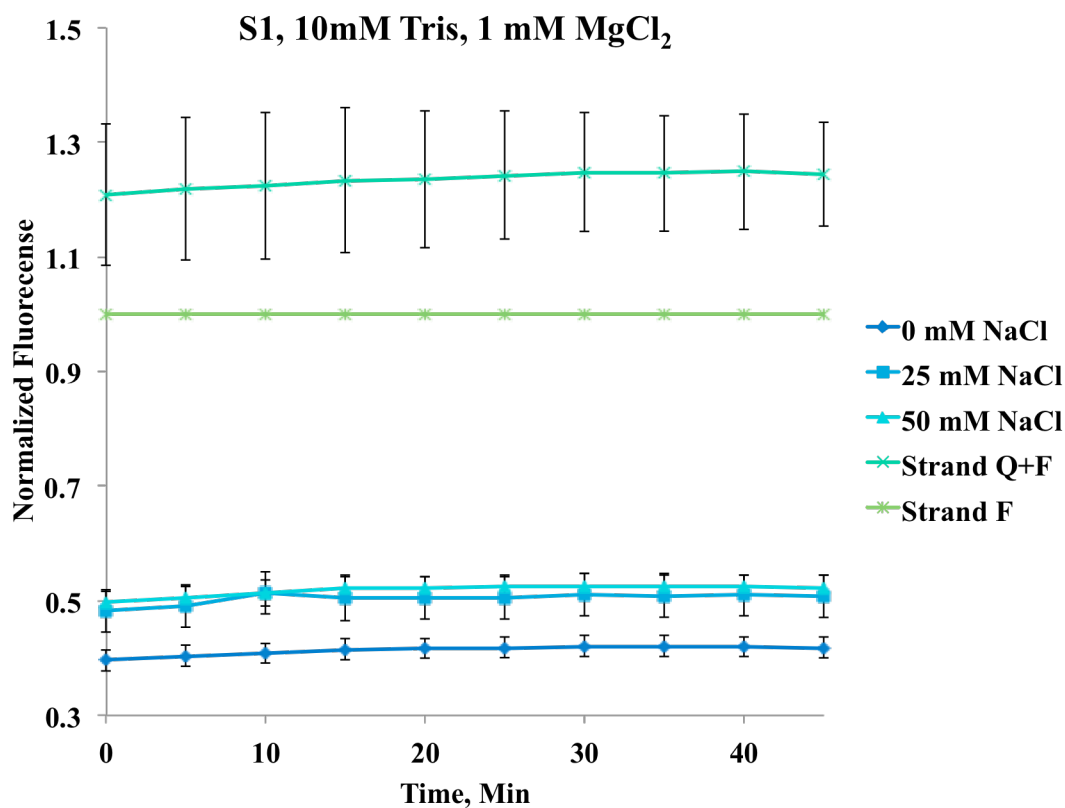


FIGURE 15. Continued.

System 2 was tested under the conditions of Trial 4 listed on Table 3. The aptamer complex was hybridized at the same concentration and in the same fashion as System 1. The data was represented in the same format as above. As can be seen by Figure 16, System 2 was able to hybridize much more efficiently, showing 10-fold quenching (approximately 0.09 NF) at all salt concentrations after accounting for standard deviation. The control containing Strand F and Q also fluoresced at higher NF than the F strand alone.

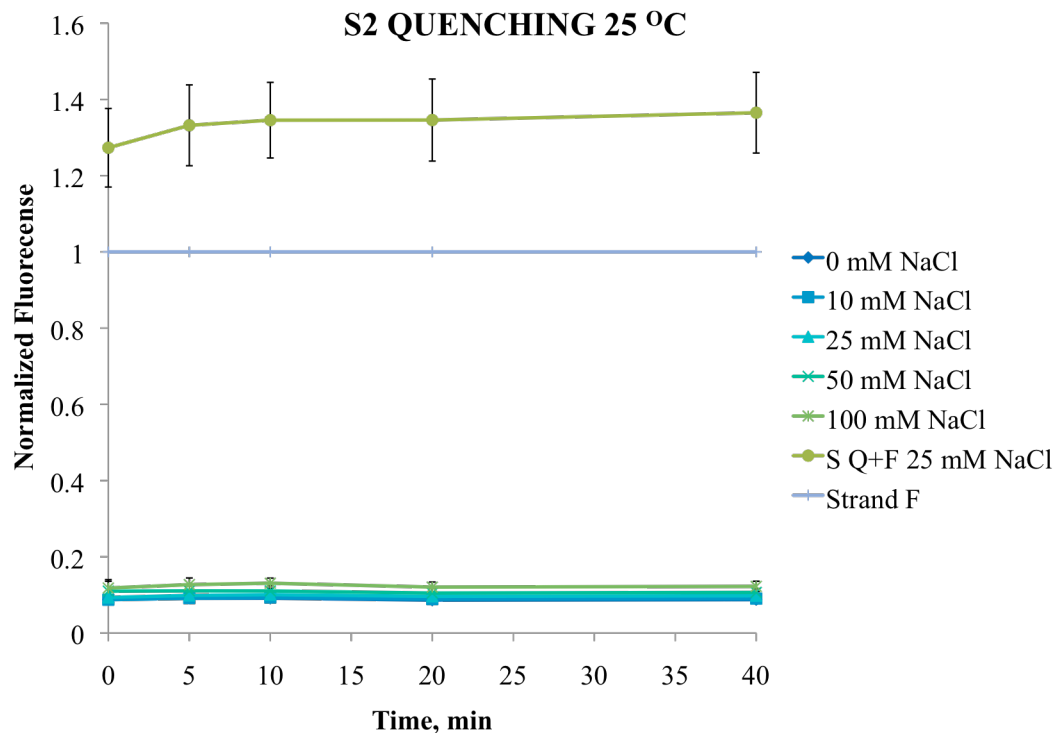


FIGURE 16. Quenching of System 2. System 2 at various NaCl concentrations at 1 mM of $MgCl_2$ and 10 mM Tris. Each data point is an average of 5 readings. Error bars indicate the standard deviation between readings.

As System 2 was observed to be able to hybridize at higher percentage than System 1, it was chosen to be further tested in order to fulfill the aims set in Section 2.1.

2.3. TEMPERATURE DEPENDENCE OF SYSTEM 1 AND SYSTEM 2

In order to determine if System 2 could form and remain stable at physiological temperatures, the thermal stability of the complex was studied by heating it beyond 37 °C and determining the experimental melting temperature. The results of these studies ensured that our aptamer system would dissociate as projected.

2.3.1. MATERIALS AND METHODS

The aptamer complex was annealed together in the same fashion as in Section 2.2.1 in a buffer with 1 mM MgCl₂ and 10 mM Tris at pH 7.4 at 0 or 50 mM NaCl concentrations. Controls were prepared as previously mentioned. DNA was heated in microplate reader to 37, 45, 50, 55, and 60 °C and was allowed to equilibrate for 30 minutes at each temperature before fluorescence readings were taken.

2.3.2. RESULTS AND DISCUSSIONS

As can be seen from Figure 17, System 2 was able to quench to the same extent as reported above at 25 °C. Although there is minimal increase in NF at 37 °C, the quenching is still in the magnitude of 10-fold compared to the sample containing Strand F alone. At 45 °C we detect a small increase in NF from the starting value at 25 °C. As the temperature approaches 50 °C we see a large NF increase. The NF at this temperature jumps to approximately 50 % NF reported for strand F. For this reason we could assume that the experimental T_m for this complex is near 50 °C at both 0 nM and 50 nM NaCl concentrations. Beyond 60 °C, NF is detected similar to the control containing both strands F and Q.

Based on the experimental results, System 2 fulfills the specific aims that were set in section 2.1:

1. The aptamer complex must not include palindromes or sequences that would cause the aptamer complex strands to anneal to themselves or in a fashion that was unwanted.

2. Aim two is that the proposed conformations would allow the complementary strands (F and Q) to anneal to the elongated aptamer strand (L) with enough affinity and fidelity to form a strong crosslink and, in the process, quench the fluorescence molecule to enable monitoring of the complexation status.
3. Aim three is that the complementary strands would anneal at varying affinities and strength.

Since system two proved to meet these criteria, System 1 complex was then tested for response to VEGF protein.

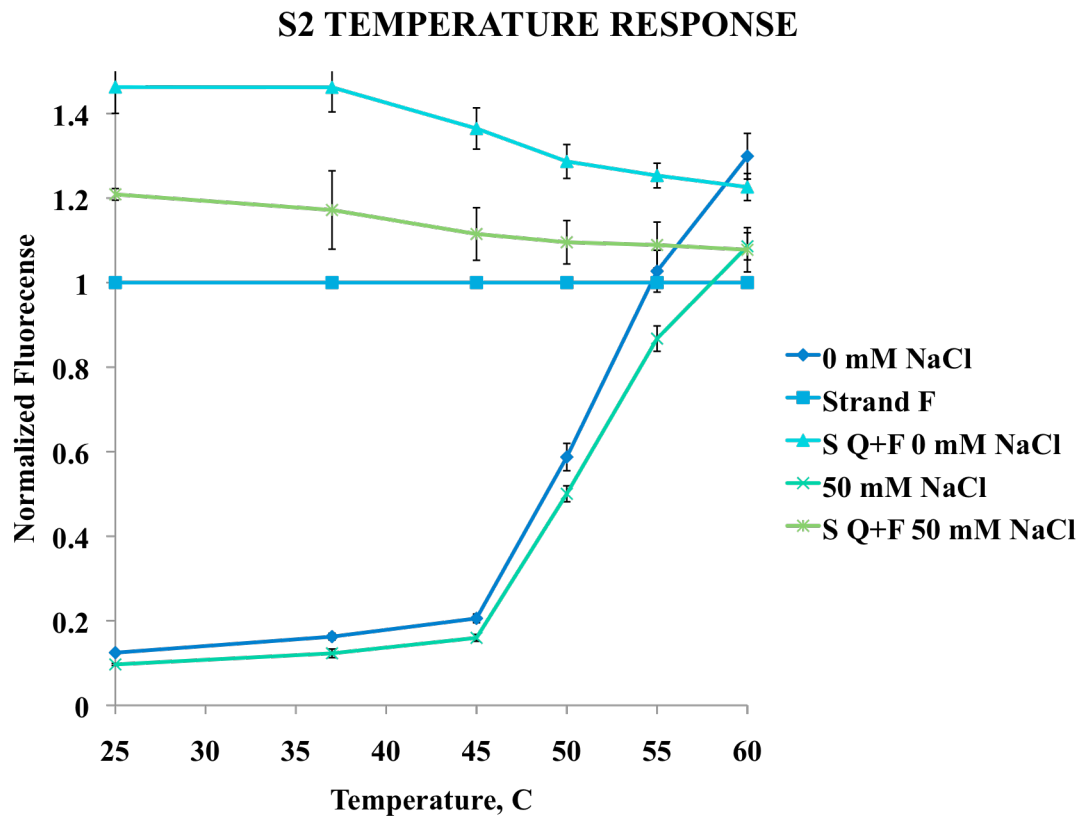


Figure 17. Temperature response of system 2. Each data point is an average of 5 readings. Error bars indicate the standard deviation.

2.4. SYSTEM 2 RESPONSE TO VEGF

The previous sections dealt with the selection of aptamer extension and complementary strand sequences to enable the formation of a complex that could be used as a molecularly responsive crosslinker, and with the evaluation of the ability of these sequences to form the expected hybridized complex. The final step in the characterization of this complex was to study its ability to respond to (i.e. be disrupted by) the target molecule VEGF.

2.4.1. MATERIALS AND METHODS

The aptamer complex was prepared, annealed, and plated on 7 rows of a 384 plate with 5 repetitions per condition. Quenching was determined in the same fashion as above. VEGF was purchased (Biolegend, San Diego, CA) and was placed in a buffer containing 10 mM tris and 1 mM MgCl₂ at a concentration of 500 nM and stored at -25 °C. The aptamer complexes were monitored for 30 min before adding 20 µL of increasing VEGF concentrations of 0 nM, 1 nM, 10 nM, 25 nM, 50 nM, 75 nM, and 100 nM to each well. A control with strand F only was also prepared as stated in Section 2.1. This control was subjected to 25 nM of VEGF. The fluorescence was taken every 5 minutes for 45 minutes.

2.4.2. RESULTS AND DISCUSSIONS

The resulting data is graphed in Figure 18. The aptamer complex successfully responded to the VEGF protein and dehybridized at all VEGF concentrations. The response of the aptamer towards the VEGF was immediate, as seen in Figure 18. The

aptamer complex that received no VEGF did increase NF, but was still below what was observed when VEGF was added. Of note is that when higher concentrations of VEGF were used it was observed that the NF was lower than when lower concentrations of VEGF were used. This is counterintuitive since more VEGF should produce a higher extent of complex disruption and, therefore, higher NF from the disruption of the quenching process. However, the formulation of the VEGF, as purchased, includes high concentrations of monovalent and divalent ions that likely stabilize the aptamer complex. As the concentration of cations increase, it is possible that the aptamer complex becomes more stable. In addition, previous reports state that the dissociation constant (K_D) of the VEGF protein to the aptamer increases from 1 nM at 0 mM NaCl to 1000 nM at 250 mM NaCl [122]. Thus, increasing salt concentrations coming from the VEGF solution would have led to a lower affinity of the aptamer to the VEGF protein.

S2 VEGF RESPONSE

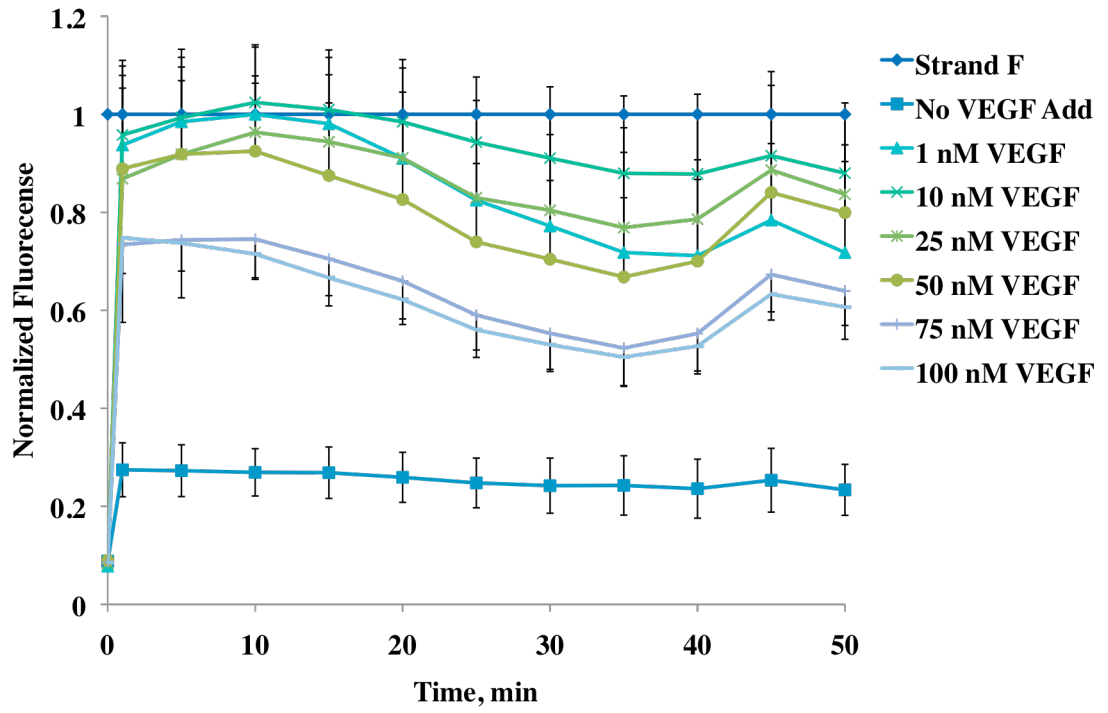


FIGURE 18. Aptamer complex response to VEGF. Each data point is an average of 5 readings. Error bars indicate the standard deviation.

3. HYDROGEL SYNTHESIS USING PEG CROSSLINKER

As previously mentioned, the overall goal of this project is to prepare molecularly responsive hydrogels that can be prepared in the presence of live cells and that incorporate aptamer complexes to provide molecularly controlled biodegradability. In order to achieve this, Chapter 2 described the considerations taken into the design and testing of an aptamer complex. Chapter 3 focuses on the development of copper-free click chemistry for the preparation of the hydrogels under mild conditions, but with the use of a bifunctional PEG-azide as a substitute crosslinker in lieu of the much more expensive aptamer complex. This work enabled the determination of proper synthetic protocols that could later be used for preparation of the molecularly responsive hydrogels in future work.

3.1. DBCO SYNTHESIS

3.1.1. MATERIALS AND METHODS

Dibenzylcyclooctyne (DBCO) synthesis was conducted in collaboration with Dr. Shiva Rastogi and Dr. William Brittain. The synthesis was carried out through five major steps [159]. Step 1 initiated the reaction by adding 2.22 mL of liquid phenylacetaldehyde (Sigma Aldrich) equaling 20 mmole to a three-neck round-bottom flask. A volume of 10 mL of anhydrous chloroform was added to the round bottom flask. The solution was chilled to 0 °C for 30 min. A volume of 313 μ L of iodotrimethylsilane (Me_3SiI) was added to the solution, followed by the addition of 40 mL of anhydrous chloroform. The mixture and allowed to react at 4 °C for seven days. After the reaction, the solution was

washed using 0.1 M HCl followed by washes with water and brine to remove byproducts. The remaining organic solution was dried using anhydrous MgSO_4 and the solution was concentrated through the use of a rotary evaporator. The product of Step 1 was dissolved in enough CH_2Cl_2 and purified via chromatography in a silica gel column using a 2 % ethyl acetate/hexane mobile phase. The reaction was evaluated by thin layer chromatography using 5% ethyl acetate/hexane mobile phase.

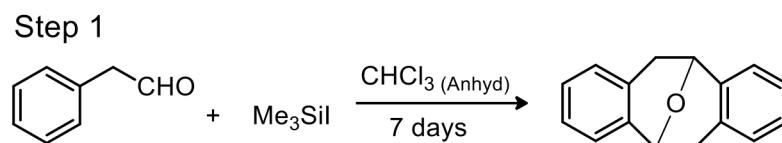


FIGURE 19. Step one of DBCO synthesis.

Step 2, as illustrated by Figure 20, was conducted by dissolving the concentrated sample in 5 mL of dry THF in a 50 mL round bottom flask. A total of 2.5 mole of *n*-Butyllithium was used per mole of product from Step 1. The reaction was allowed to occur for four hours. After the four hours the products were washed using H_2O and brine. The organic solution was separated and anhydrous MgSO_4 was used to remove remaining water. The organic layer was concentrated and purified by gravity chromatography using a silica gel with a 2.5% ethyl acetate/hexane mobile phase. The desired product was detected by thin layer chromatography using a 5% ethyl acetate/hexane mobile phase. The product was then concentrated once more.

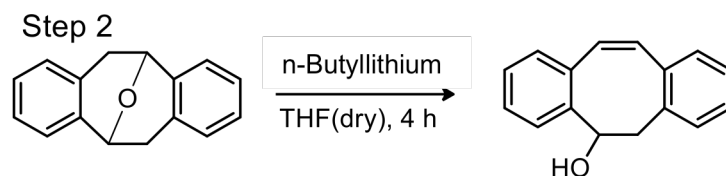


FIGURE 20. Step two of DBCO synthesis. A hydroxyl group is produced in order to provide a means for modification.

The concentrated sample was dissolved in 20 mL of CHCl_3 in a 100 mL round bottom flask. In Step 3, a 1:1 molar ratio of product to Br_2 was added drop wise under nitrogen gas to the round bottom flask and allowed to react for one hour (Figure 21). As before, the product was washed, separated by gravity chromatography (2.5% ethyl acetate/hexane), and detected by thin layer chromatography (10% ethyl acetate/hexane). The product was concentrated once more.

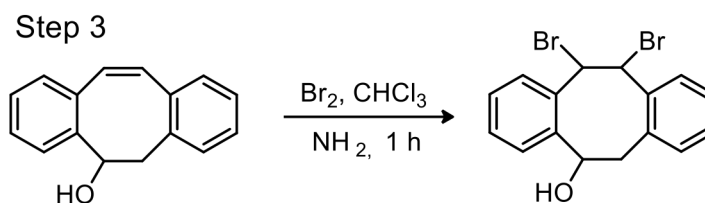


FIGURE 21. Step three of DBCO synthesis. Cyclooctene ring is brominated.

Finally, for Step 4, lithium diisopropylamide (LDA) was prepared *in situ* by combination of 3 mL of diisopropylamine and 15 mL of *n*-butyllithium in a round bottom flask. As shown in Figure 22, the product of step three was dissolved in 20 mL of THF. To this solution, 15 mL of LDA was added and the mixture was allowed to react for 1 hr at 0 °C. The reaction was allowed to proceed for additional 2 hours. The product was then washed, isolated, and detected as in step 2.

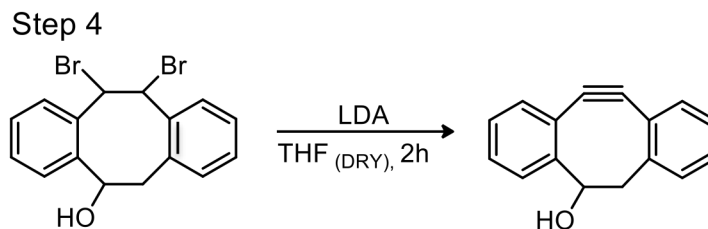


FIGURE 22. Step four of DBCO synthesis. Bromine is removed in order to yield a cyclooctyne ring.

In Step 5 the DBCO was functionalized with 4-nitrophenyl carbonochloridate (in DCM) by dissolving the product from Step 4 in dry DCM and adding Pyridine, as seen in Figure 23. The resulting product was then characterized via UV-vis absorbance spectroscopy using a Biotek plate reader and through nuclear magnetic resonance (NMR) (Varian 400 MHz FT NMR).

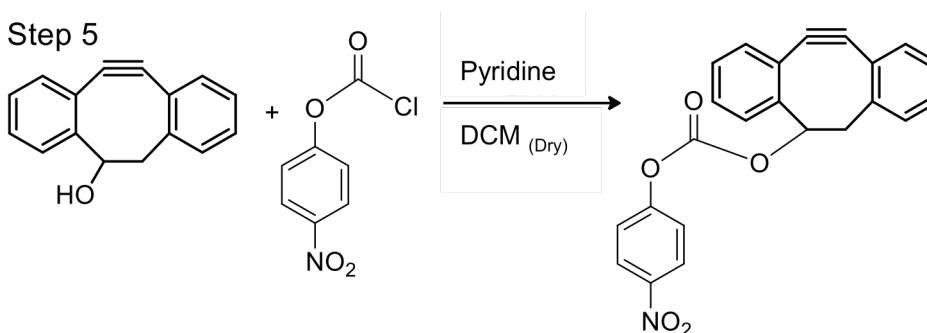


FIGURE 23. Step five of DBCO synthesis. Preparation of nitrophenyl ester of DBCO.

3.1.2. RESULTS AND DISCUSSIONS

Resulting data from UV-Vis absorption spectroscopy is plotted in Figure 24. The graph clearly shows the two-indicative peaks attributed to DBCO near 290 and 305 nm Range. The two absorption peaks are attributed to the benzul ring and octyne group. Carbon-13 NMR was used to confirm the structure of DBCO The experimental spectra (Figure 25 A) show that the compound was indeed formed.

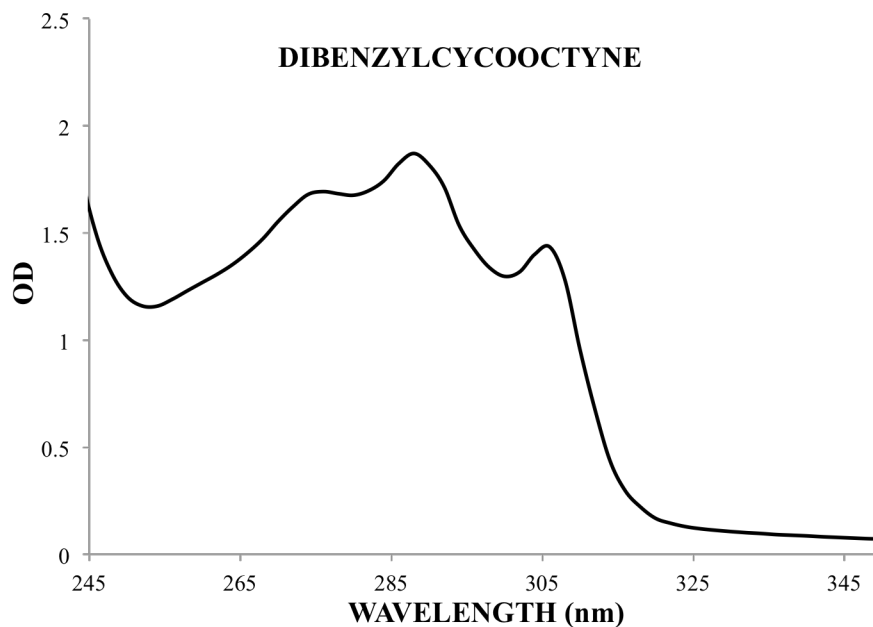


FIGURE 24. DBCO UV-vis absorption.

3.2. PEG-DBCO CONJUGATION

Hydrogels were synthesized through the use of copper-free click chemistry. Specifically, as shown in Figure 1, hydrogel synthesis was carried out by the reaction of at least two building blocks: DBCO-functionalized four-arm poly(ethylene glycol) (PEG) and a bifunctional crosslinker that would eventually be an aptamer complex, but, in this chapter, was substituted with a bifunctional PEG azide. In addition to these two building blocks, a future goal was to also incorporate cell-adhesion peptides based on the RGD amino acid sequence. However, this will be explored in future work.

The reaction between the two building blocks involved the (3 + 2) cycloaddition between an azide and DBCO to crosslink the hydrogel together.

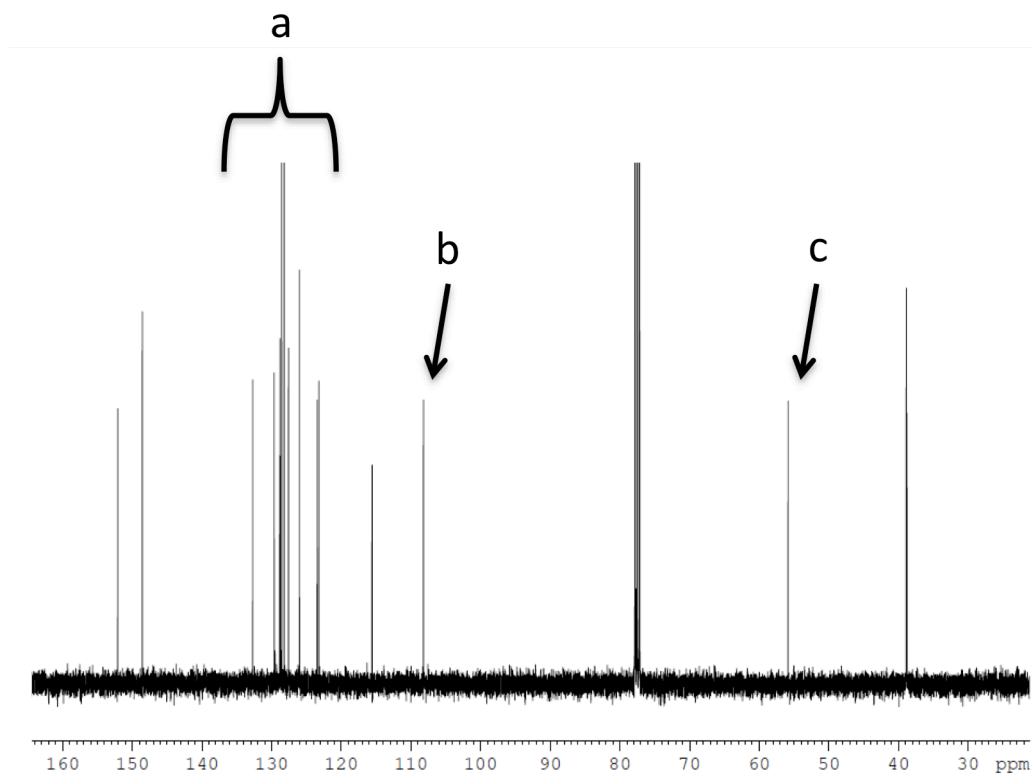


FIGURE 25. Carbon-13 NMR of DBCO molecule. a) region belonging to aromatic region of DBCO b) is region belonging to alkyne group c) is the peak belonging to the carbon bonded to the OH group.

3.2.1. MATERIALS AND METHODS

The nitrophenyl-functionalized DBCO was used to end-functionalize a 20 kDa MW four-arm PEG-amine (Laysan Bio, Inc., Arab, AL). The reaction results in the formation of a physiologically stable amide bond between each end of the four-arm PEG and DBCO. After dissolving the DBCO and PEG separately in DCM, DBCO was added to the PEG solution at a 1:1.2 mole equivalency in the presence of triethylamine. The mixture was allowed to react for 24 hours, after which it was washed with water and brine and dried over anhydrous sodium sulfate. The resulting green oil was purified by

gel chromatography using a 2.5% ethyl acetate/hexane solvent system as mobile phase. The polymer further purified by precipitating it using cold diethylether (Fisher Scientific) and centrifuged (Beckman Coulter Avanti J26-XP) at 12,500 x g. Cycles of pellet dissolution in chloroform, precipitation, and pellet collection were repeated three times to remove excess unbound DBCO. NMR spectroscopy and UV-Vis were conducted to characterize the functionalized polymer.

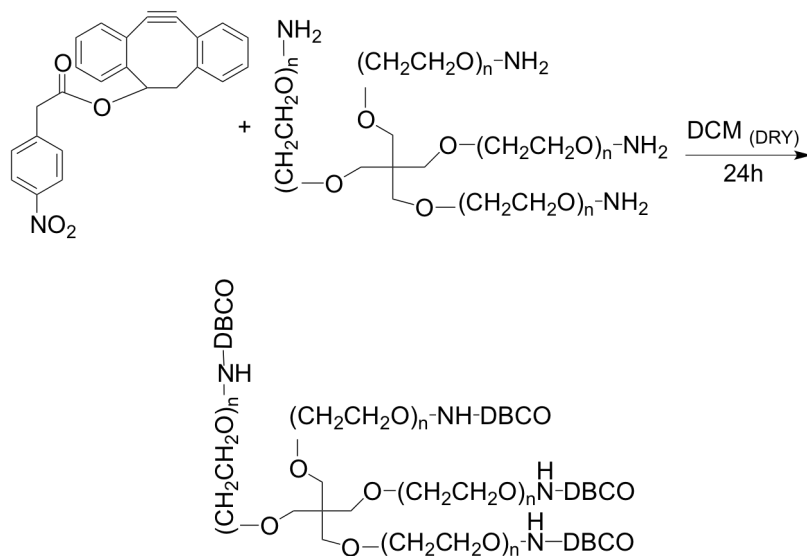


FIGURE 26. DBCO addition to PEG-NH₂.

3.2.2. RESULTS AND DISCUSSIONS

Absorption spectra were obtained for the PEG-DBCO samples as shown in Figure 26. The presence of peaks at 290 and 305 nm confirmed the attachment of DBCO to the 4-arm PEG.

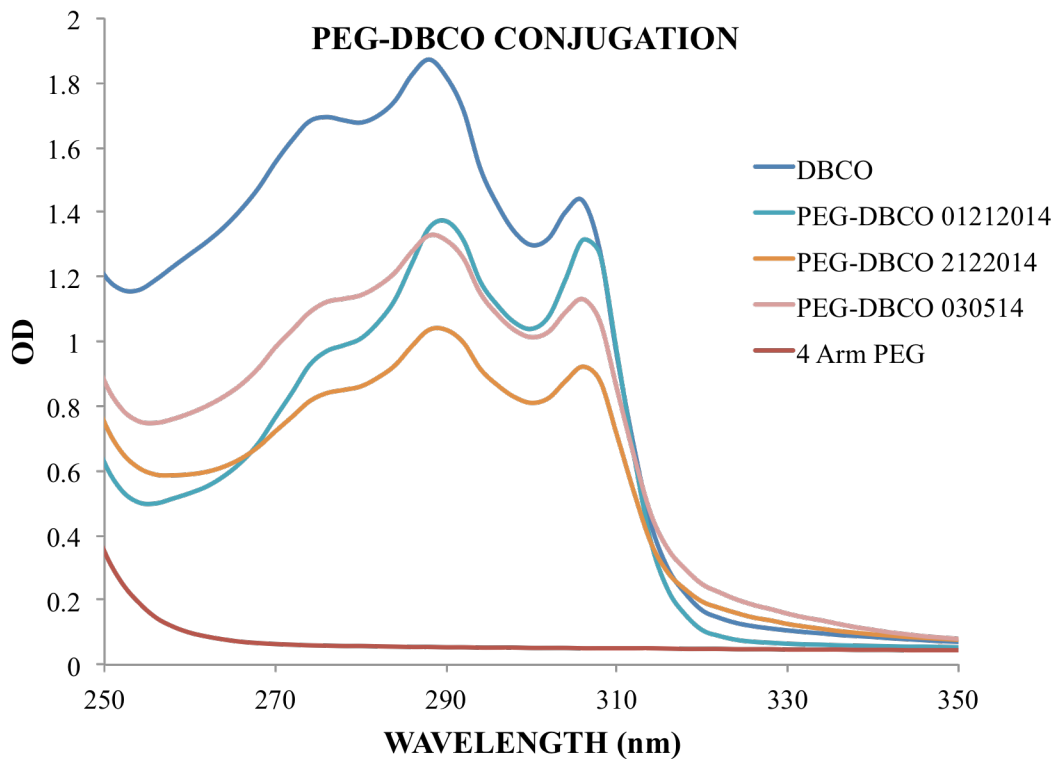


FIGURE 27. Absorption spectra of PEG-DBCO.

Figure 28 shows the carbon NMR spectra for the DBCO-functionalized PEG. The proton atoms of PEG show a peak at 3.6 ppm. This was confirmed in separate NMR studies with the 4-arm PEG reagent used in the synthesis. The NMR spectra confirmed that the PEG had been functionalized.

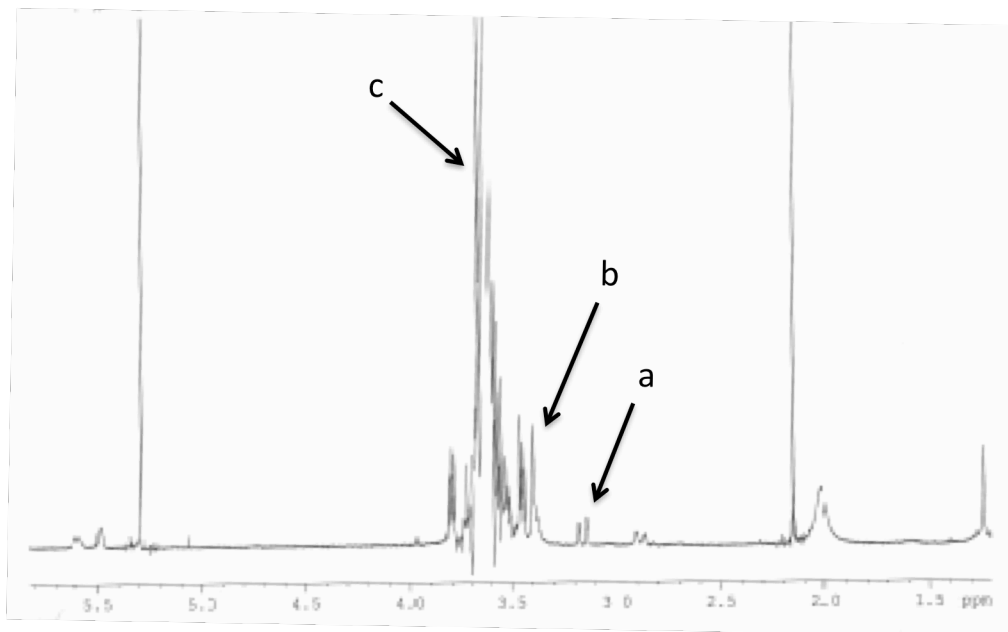


FIGURE 28. Experimentally derived Proton NMR spectra of PEG-DBCO. Point a and b are the indicative peaks of DBCO. Peak c is indicative of PEG.

3.3. HYDROGEL SYNTHESIS

In order to determine whether the four-arm PEG-NH₂ had been functionalized with enough DBCO to enable the preparation of an insoluble hydrogel network, a substitute bifunctional azide-functionalized PEG (azide-PEG-azide) was used to prepare a hydrogel.

3.3.1. MATERIALS AND METHODS

Four-arm PEG-DBCO was dissolved to 10% in dimethyl sulfoxide (VWR) by heating the polymer to 45 °C and using sonication (Fisher Scientific Model 500 Sonicator). The crosslinker substitute, azide-PEG-Azide (5,000 Da, Sigma Aldrich) was dissolved in deionized water (Millipore Direct-Q3 UV Water Purification System). The polymers were mixed (1:4 molar ratio of 4-arm PEG DBCO to azide-PEG-azide) into a 7 mL vial and the volume was adjusted to 8-10 % weight of polymer to volume. This dilution resulted in a total DMSO content of 41.5% v/v with respect to water. The polymers were

allowed to react overnight at 37 °C in a cell culture incubator. It should be noted that live, cultured human cancer cells are routinely exposed to 5% DMSO aqueous solutions as a cryopreservative. However, higher DMSO concentrations will not be suitable for incorporation of live cells within the hydrogel matrix. Unfortunately, the solubility of the DBCO-functionalized PEG in water was not sufficient to enable the use of a lower volume of DMSO. Future studies will look at methods for increasing the solubility of this building block and testing the encapsulation of cells.

3.3.2. RESULTS AND DISCUSSIONS

The functionalized PEG-DBCO was able to successfully click with the substitute crosslinker. The hydrogel was formed using 15 mg of PEG-DBCO and 13.9 mg of PEG-azide. The resulting hydrogel was then washed with water and freeze dried. The dried matrix weighed 19.7 mg. As can be seen in Figure 29A, the hydrogel has a small percentage of loosely bound polymers that weren't able to crosslink as desired. Upon rehydration in excess water, the freeze-dried matrix was able to regain its mechanical properties thus confirming that the material was in fact an insoluble hydrogel and not simply a mixture of polymers. The hydrogel reabsorbed large amounts of water, making it translucent as shown in Figure 29C. Although the molar ratio of polymer to DBCO needs to be optimized to yield maximum crosslinking, the functionalized PEG-DBCO proved to be functionalized to a high degree in order to create a matrix.

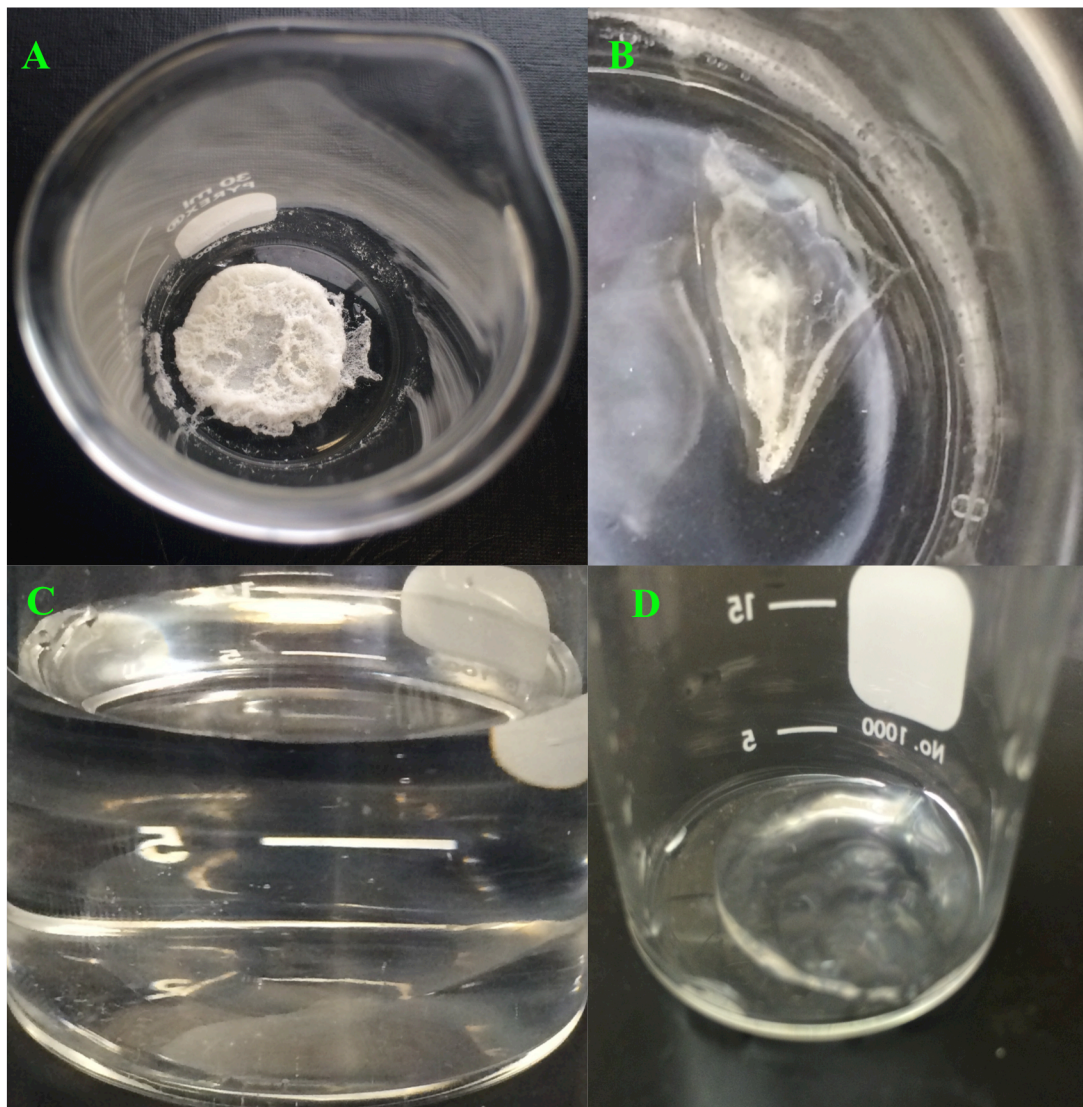


FIGURE 29. Hydrogel synthesis using PEG-azide substitute crosslinker. A) Freeze dried sample. B) Image of hydrogel 5 min after adding it to 10 mL of D₂O. C) Image of hydrogel 1 h after submerging it in water. D) Excess water was removed 4 hours later, demonstrating the presence of an insoluble hydrogel network.

4. CELL ADHESIVE PEPTIDE

4.1. CYCLO ARGININE GLYCINE ASPARTIC ACID SYNTHESIS

A mimicry peptide was synthesized in order to allow the anchoring of the cells to the hydrogel. The mimicry peptide consists of a ten amino acids with the sequence Lysine-Lysine-Serine-Serine-Serine-Phenylalanine-Glutamic Acid-Aspartic Acid-Glycine-Arginine (L-L-S-S-S-F-E-D-G-R). The cyclization occurs between the Arginine and Glutamic Acid with the remaining amino acids serving as an extension (S-S-S) and sites for further chemistry (L-L) [160].

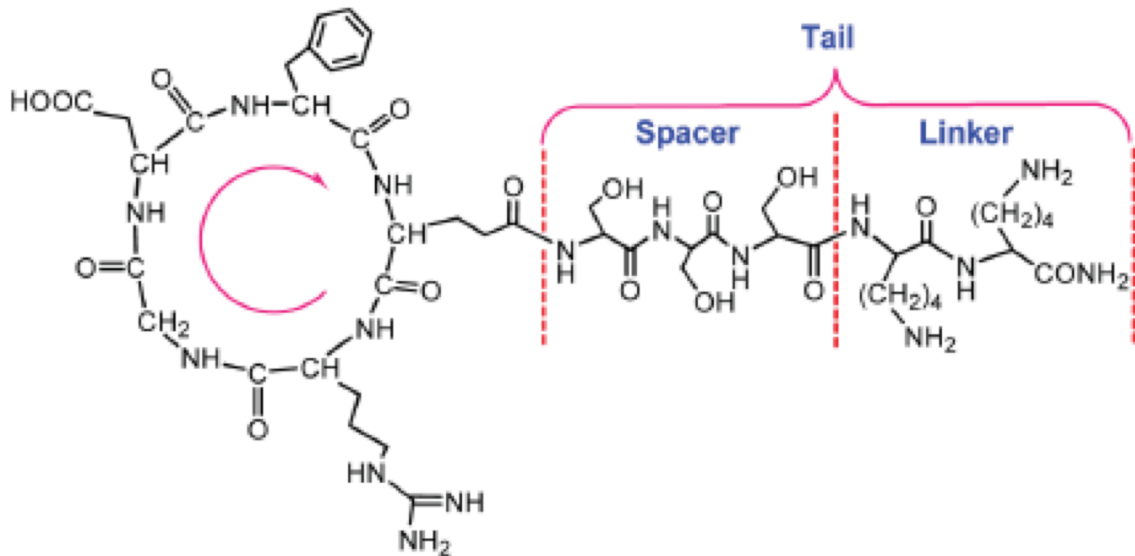


FIGURE 30. Structure of cRGD peptide. Linker is made from L-L amino acids. Spacer is made from S-S-S amino acids. The cyclization is formed using EFDGR amino acids.

4.1.1. MATERIALS AND METHODS.

The amino acids (L, S, E, F, D, G, R) were protected at the carboxylic acid position with protective group Fluorenylmethyloxycarbonyl chloride (Fmoc) (AnaSpec). *O*-tert-butyl (tBu) was used as protective groups for residue groups of Aspartic Acid and Serine amino acids (AnaSpec). Glutamic acid residue was protected with allyl group. Arginine (AnaSpec) was protected with 2,2,4,6,7-pentamethyldihydrobenzofuran-5-sulfonyl (Pbf). *O*-tert-butoxycarbonyl was used to protect lysine amino acid residues. The synthesis of the mimicry peptide was carried out through solid face synthesis using Fmoc-aminomethyl-3,5-dimethoxyphenoxy-valeric acid (Pal) resin (AnaSpec) (loaded at 0.6 mmol/g). Addition of the amino acids was carried out through the use of *O*-(benzotriazol-1-yl)-*N,N,N',N'*-tetramethyluronium hexafluorophosphate (HBTU) (Sigma-Aldrich), and 1-hydroxybenzotriazole (HOBt) (Sigma-Aldrich) and *N,N*-diisopropylethylamine (DIPEA) (Sigma-Aldrich). Addition of the amino acids was carried out by first soaking the resin in 2 mL of DMF for four hours under N₂. Following the soaking and before the addition of the first amino acid the Pal resin was deprotected by the following steps: addition of 1 mL of piperidine/DMF solution (1:4 respectively) for three minutes, then washing with 1 mL of DMF two times, treating with 1 mL of piperidine/DMF solution for three minutes, and then washing with DMF and DCM (these steps were used to remove Fmoc and tBu groups). Coupling of the amino acids occurred by adding 0.5mmol HOBt, 0.49 mmol HBTU, 1 mmol DIPEA for every 0.5 mmol of the amino acid added. The reaction was allowed to proceed for 4 hours under N₂.

Following the peptide synthesis, the Fmoc group on the *N*-terminus of the arginine

amino acid was removed addition of 20% (v/v) piperidine in DMF for 10 minutes. This was followed by the removal of the allyl group on the glutamic acid through the use of three mole equivalent of tetrakis(triphenylphosphine)palladium(0) ($\text{Pd}(\text{PPh}_3)_4$) (Sigma Aldrich) (in respect to loading number) and 20% (v/v) piperidine in DMF for 10 min. Cyclization was carried out by addition of 1-Hydroxy-1-azabenzotriazole uronium (HATU) (VWR) in N_2 and allowing to react overnight.

The peptide was then cleaved by the following steps: 1) washing four times with 1 mL of H_2O , methanol, acetone and DCM; 2) draining the resin and adding 1.5 mL of TFA/ H_2O solution (95/5) and allowing to react for 3 hours under N_2 ; 3) draining the resin and washing with TFA/ H_2O solution and allowing the peptide to drain into a vial; 4) precipitation of the peptide with ice cold diethyl ether; 5) centrifugation and lyophilization of the precipitate. The resulting product was analyzed using MALDI-TOF with the peptide matrix 2,5-dihydroxybenzoic acid utilizing the sandwich method. The matrix consisted of a saturated solution of 2,5-dihydrobenzoic acid in 50/50 water/acetonitrile solution, while the peptide was dissolved at 10 pM in this same solvent system.

4.1.2. RESULTS AND DISCUSSIONS

The theoretical MW of the peptide was calculated to be 1,139 Da. MALDI-TOF spectrum shows the major product obtained to be at a MW of 1135 Da. Based on the spectrum we could conclude that the product was successfully synthesized. HPLC needs to be carried out in order to remove impurities.

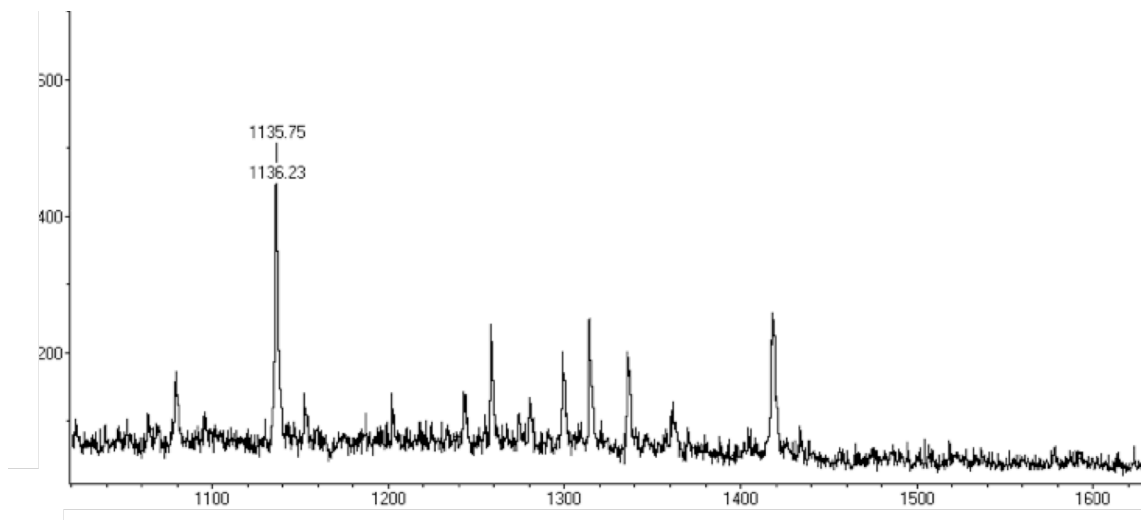


FIGURE 31. MALDI-TOF spectrum of cRGD peptide. The major product corresponding to the peptide sequence is labeled at 1135.75 Da.

5. SUMMARY AND CONCLUSIONS

The overall goal of the project was to create a molecularly responsive hydrogel through the use of copper-free click chemistry for cell culture. In this work, three fundamental aims were accomplished in support of the overall project: the formation of a hydrogel through the use of copper-free click chemistry, the development of the aptamer complex, and the synthesis of the peptide for cell adhesion to the hydrogel.

The design of the aptamer complex was aided through *in silico* testing using IDT OligoAnalyzer 3.1 in order to estimate the T_m for each oligonucleotide and thereby induce the expected stability of the hybrid. *In vitro* studies were used to determine the aptamers binding affinity at varying salt concentrations, experimental determination of melting temperature, and response to VEGF protein. The aptamer complex was shown to effectively function and achieve the aims set in 2.1. However, further studies need to be carried out to determine the cause for higher observed normalized fluorescence of strand Q and F compared to that of control strand F. The aptamer complex should also be tested for response towards VEGF at higher salt and VEGF concentrations.

Within the aim of the hydrogel formation there were three specific tasks that needed to be accomplished:

1. The synthesis, functionalization, and characterization of DBCO molecule.
2. The conjugation, purification, and characterization of DBCO-functionalized 4-arm PEG to form PEG-DBCO.
3. Crosslinking the PEG-DBCO with an azide functionalized linear PEG.

The role of the PEG-azide is to be a substitute for aptamer complex. Through the use of the substitute crosslinker we verified that the PEG has been efficiently functionalized. The work presented here shows that the DBCO molecule and that PEG-DBCO were efficiently formed and characterized. Further studies should focus on decreasing the volume of DMSO used to dissolve the PEG-DBCO from 40.5% to less than 5%.

As part of the project a cRGD was synthesized using solid phase synthesis in order to serve as a molecular anchor, annealing the cells to the matrix. The peptide was characterized using MALDI-TOF and showed to have cyclized. Future studies should focus on conjugating the peptide to a COOH-PEG-azide in order to click the peptide onto the matrix. In addition, an oligonucleotide was end functionalized with azides at 5' and 3' prime positions in order to serve as a crosslinker for hydrogel synthesis. Future studies will focus on hydrogel formation using this oligomer. Characterization of the hydrogel should follow characterization by scanning electron microscopy, atomic force microscopy, and confocal microscopy. Incorporation of the aptamer complex should follow along with similar characterization. Finally inclusion of mammalian cells will be utilized to prove the efficacy of the matrix as a cell-culture model.

REFERENCES

1. Thiel, W.H., T. Bair, K. Wyatt Thiel, et al., *Nucleotide bias observed with a short SELEX RNA aptamer library*. *Nucleic Acid Ther*, 2011. **21**(4): p. 253-263.
2. Potty, A.S., K. Kourentzi, H. Fang, et al., *Biophysical characterization of DNA aptamer interactions with vascular endothelial growth factor*. *Biopolymers*, 2009. **91**(2): p. 145-156.
3. Hoeben, A., B. Landuyt, M.S. Highley, et al., *Vascular endothelial growth factor and angiogenesis*. *Pharmacol Rev*, 2004. **56**(4): p. 549-580.
4. Himo, F., T. Lovell, R. Hilgraf, et al., *Copper(I)-catalyzed synthesis of azoles. DFT study predicts unprecedented reactivity and intermediates*. *J Am Chem Soc*, 2005. **127**(1): p. 210-216.
5. Baird, A. and N. Ling, *Fibroblast growth factors are present in the extracellular matrix produced by endothelial cells in vitro: implications for a role of heparinase-like enzymes in the neovascular response*. *Biochem Biophys Res Commun*, 1987. **142**(2): p. 428-435.
6. Berthiaume, F., T.J. Maguire, and M.L. Yarmush, *Tissue engineering and regenerative medicine: history, progress, and challenges*. *Annu Rev Chem Biomol Eng*, 2011. **2**: p. 403-430.
7. Stroncek, J.D. and W.M. Reichert, *Overview of Wound Healing in Different Tissue Types*, in *Indwelling Neural Implants: Strategies for Contending with the In Vivo Environment*, W.M. Reichert, Editor. 2008: Boca Raton (FL).
8. Badylak, S.F. and R.M. Nerem, *Progress in tissue engineering and regenerative medicine*. *Proc Natl Acad Sci U S A*, 2010. **107**(8): p. 3285-3286.
9. Liu, S.Q., P.L. Ee, C.Y. Ke, et al., *Biodegradable poly(ethylene glycol)-peptide hydrogels with well-defined structure and properties for cell delivery*. *Biomaterials*, 2009. **30**(8): p. 1453-1461.
10. Schumann, D., A.K. Ekaputra, C.X. Lam, et al., *Biomaterials/scaffolds. Design of bioactive, multiphasic PCL/collagen type I and type II-PCL-TCP/collagen composite scaffolds for functional tissue engineering of osteochondral repair tissue by using electrospinning and FDM techniques*. *Methods Mol Med*, 2007. **140**: p. 101-124.
11. Porter, J.R., T.T. Ruckh, and K.C. Popat, *Bone tissue engineering: a review in bone biomimetics and drug delivery strategies*. *Biotechnol Prog*, 2009. **25**(6): p. 1539-1560.
12. Godbey, W.T. and A. Atala, *In vitro systems for tissue engineering*. *Ann N Y Acad Sci*, 2002. **961**: p. 10-26.
13. Volkmer, E., S. Otto, H. Polzer, et al., *Overcoming hypoxia in 3D culture systems for tissue engineering of bone in vitro using an automated, oxygen-triggered feedback loop*. *J Mater Sci Mater Med*, 2012. **23**(11): p. 2793-2801.
14. Hutmacher, D.W., *Scaffolds in tissue engineering bone and cartilage*. *Biomaterials*, 2000. **21**(24): p. 2529-2543.
15. Huo, D.M., F.T. Dong, W.H. Yu, et al., *Differentiation of mesenchymal stem cell in the microenvironment of retinitis pigmentosa*. *Int J Ophthalmol*, 2010. **3**(3): p. 216-219.

16. Leenman, E.E., M.S. Mukhina, M.M. Girshovich, et al., [*The place of dendritic cells in the microenvironment in Hodgkin's lymphoma*]. *Arkh Patol*, 2010. **72**(2): p. 3-7.
17. Wang, H. and L. Chen, *Tumor microenvironment and hepatocellular carcinoma metastasis*. *J Gastroenterol Hepatol*, 2013. **28 Suppl 1**: p. 43-48.
18. Nyga, A., U. Cheema, and M. Loizidou, *3D tumour models: novel in vitro approaches to cancer studies*. *J Cell Commun Signal*, 2011. **5**(3): p. 239-248.
19. Smalley, K.S., M. Lioni, K. Noma, et al., *In vitro three-dimensional tumor microenvironment models for anticancer drug discovery*. *Expert Opin Drug Discov*, 2008. **3**(1): p. 1-10.
20. Brannon-Peppas, L. and J.O. Blanchette, *Nanoparticle and targeted systems for cancer therapy*. *Adv Drug Deliv Rev*, 2004. **56**(11): p. 1649-1659.
21. Abrous, L., J. Hynes, Jr., S.R. Friedrich, et al., *Design and synthesis of novel scaffolds for drug discovery: hybrids of beta-D-glucose with 1,2,3,4-tetrahydrobenzo[e][1,4]diazepin-5-one, the corresponding 1-oxazepine, and 2- and 4-pyridyldiazepines*. *Org Lett*, 2001. **3**(7): p. 1089-1092.
22. Qiu, Y. and K. Park, *Environment-sensitive hydrogels for drug delivery*. *Adv Drug Deliv Rev*, 2001. **53**(3): p. 321-339.
23. Tokuda, E.Y., J.L. Leight, and K.S. Anseth, *Modulation of matrix elasticity with PEG hydrogels to study melanoma drug responsiveness*. *Biomaterials*, 2014. **35**(14): p. 4310-4318.
24. Dorj, B., J.E. Won, O. Purevdorj, et al., *A novel therapeutic design of microporous-structured biopolymer scaffolds for drug loading and delivery*. *Acta Biomater*, 2014. **10**(3): p. 1238-1250.
25. Thissen, H., T. Gengenbach, R. du Toit, et al., *Clinical observations of biofouling on PEO coated silicone hydrogel contact lenses*. *Biomaterials*, 2010. **31**(21): p. 5510-5519.
26. Sweeney, D.F., L. Keay, N. Carnt, et al., *Practitioner guidelines for continuous wear with high Dk silicone hydrogel contact lenses*. *Clin Exp Optom*, 2002. **85**(3): p. 161-167.
27. Stapleton, F., S. Stretton, E. Papas, et al., *Silicone hydrogel contact lenses and the ocular surface*. *Ocul Surf*, 2006. **4**(1): p. 24-43.
28. Alsberg, E., K.W. Anderson, A. Albeirutti, et al., *Cell-interactive alginate hydrogels for bone tissue engineering*. *J Dent Res*, 2001. **80**(11): p. 2025-2029.
29. Dorati, R., C. Colonna, C. Tomasi, et al., *Design of 3D scaffolds for tissue engineering testing a tough polylactide-based graft copolymer*. *Mater Sci Eng C Mater Biol Appl*, 2014. **34**: p. 130-139.
30. Yang, S., K.F. Leong, Z. Du, et al., *The design of scaffolds for use in tissue engineering. Part I. Traditional factors*. *Tissue Eng*, 2001. **7**(6): p. 679-689.
31. Lee, K.Y. and D.J. Mooney, *Hydrogels for tissue engineering*. *Chem Rev*, 2001. **101**(7): p. 1869-1879.
32. Drury, J.L. and D.J. Mooney, *Hydrogels for tissue engineering: scaffold design variables and applications*. *Biomaterials*, 2003. **24**(24): p. 4337-4351.
33. Kurzbach, D., W. Hassouneh, J.R. McDaniel, et al., *Hydration layer coupling and cooperativity in phase behavior of stimulus responsive peptide polymers*. *J Am Chem Soc*, 2013. **135**(30): p. 11299-11308.

34. Chow, D., M.L. Nunalee, D.W. Lim, et al., *Peptide-based Biopolymers in Biomedicine and Biotechnology*. Mater Sci Eng R Rep, 2008. **62**(4): p. 125-155.
35. McDaniel, J.R., J. Bhattacharyya, K.B. Vargo, et al., *Self-assembly of thermally responsive nanoparticles of a genetically encoded peptide polymer by drug conjugation*. Angew Chem Int Ed Engl, 2013. **52**(6): p. 1683-1687.
36. Liu, X., Z. Lei, F. Liu, et al., *Fabricating three-dimensional carbohydrate hydrogel microarray for lectin-mediated bacterium capturing*. Biosens Bioelectron, 2014. **58**: p. 92-100.
37. Smetana, K., Jr., M. Jelinkova, J. Vacik, et al., *Influence of intraperitoneal injection of three types of hydrogel beads on expression of carbohydrate-binding sites in spleen macrophages*. Biomaterials, 1996. **17**(24): p. 2335-2341.
38. Pussak, D., D. Ponader, S. Mosca, et al., *Mechanical carbohydrate sensors based on soft hydrogel particles*. Angew Chem Int Ed Engl, 2013. **52**(23): p. 6084-6087.
39. Pussak, D., D. Ponader, S. Mosca, et al., *Specific Adhesion of Carbohydrate Hydrogel Particles in Competition with Multivalent Inhibitors Evaluated by AFM*. Langmuir, 2014.
40. He, X., B. Wei, and Y. Mi, *Aptamer based reversible DNA induced hydrogel system for molecular recognition and separation*. Chem Commun (Camb), 2010. **46**(34): p. 6308-6310.
41. Zhang, L., J. Lei, L. Liu, et al., *Self-assembled DNA hydrogel as switchable material for aptamer-based fluorescent detection of protein*. Anal Chem, 2013. **85**(22): p. 11077-11082.
42. Hoffmann, C., S. Schuller-Petrovic, H.P. Soyer, et al., *Adverse reactions after cosmetic lip augmentation with permanent biologically inert implant materials*. J Am Acad Dermatol, 1999. **40**(1): p. 100-102.
43. Imran ul-haq, M., J.L. Hamilton, B.F. Lai, et al., *Design of long circulating nontoxic dendritic polymers for the removal of iron in vivo*. ACS Nano, 2013. **7**(12): p. 10704-10716.
44. Ornelas-Megiatto, C., P.R. Wich, and J.M. Frechet, *Polyphosphonium polymers for siRNA delivery: an efficient and nontoxic alternative to polyammonium carriers*. J Am Chem Soc, 2012. **134**(4): p. 1902-1905.
45. Usher, F.C., J.E. Allen, Jr., R.W. Crosthwait, et al., *Polypropylene monofilament. A new, biologically inert suture for closing contaminated wounds*. JAMA, 1962. **179**: p. 780-782.
46. Dvali, M.L. and G.G. Ziangirova, *[Use of biologically inert metals for artificial eye lens bases (experimental study)]*. Vestn Oftalmol, 1976(4): p. 46-48.
47. Kim, Y., S. Binauld, and M.H. Stenzel, *Zwitterionic guanidine-based oligomers mimicking cell-penetrating peptides as a nontoxic alternative to cationic polymers to enhance the cellular uptake of micelles*. Biomacromolecules, 2012. **13**(10): p. 3418-3426.
48. Murthy, N., J. Campbell, N. Fausto, et al., *Bioinspired pH-responsive polymers for the intracellular delivery of biomolecular drugs*. Bioconjug Chem, 2003. **14**(2): p. 412-419.
49. de Las Heras Alarcon, C., B. Twaites, D. Cunliffe, et al., *Grafted thermo- and pH responsive co-polymers: surface-properties and bacterial adsorption*. Int J Pharm, 2005. **295**(1-2): p. 77-91.

50. Kanekiyo, Y., R. Naganawa, and H. Tao, *pH-responsive molecularly imprinted polymers*. *Angew Chem Int Ed Engl*, 2003. **42**(26): p. 3014-3016.
51. Park, I.K., K. Singha, R.B. Arote, et al., *pH-Responsive Polymers as Gene Carriers*. *Macromol Rapid Commun*, 2010. **31**(13): p. 1122-1133.
52. Alexander, C., *Temperature- and pH-responsive smart polymers for gene delivery*. *Expert Opin Drug Deliv*, 2006. **3**(5): p. 573-581.
53. Schmaljohann, D., *Thermo- and pH-responsive polymers in drug delivery*. *Adv Drug Deliv Rev*, 2006. **58**(15): p. 1655-1670.
54. Betancourt, T., J. Pardo, K. Soo, et al., *Characterization of pH-responsive hydrogels of poly(itaconic acid-g-ethylene glycol) prepared by UV-initiated free radical polymerization as biomaterials for oral delivery of bioactive agents*. *J Biomed Mater Res A*, 2010. **93**(1): p. 175-188.
55. Mori, T., S. Beppu, M.R. Berber, et al., *Design of temperature-responsive polymers with enhanced hysteresis: alpha,alpha-disubstituted vinyl polymers*. *Langmuir*, 2010. **26**(12): p. 9224-9232.
56. Lin, S.C., K.L. Lin, H.C. Chiu, et al., *Enhanced protein renaturation by temperature-responsive polymers*. *Biotechnol Bioeng*, 2000. **67**(5): p. 505-512.
57. Park, S., M. Zhong, T. Lee, et al., *Modification of the surfaces of silicon wafers with temperature-responsive cross-linkable poly[oligo(ethylene oxide) methacrylate]-based star polymers*. *ACS Appl Mater Interfaces*, 2012. **4**(11): p. 5949-5955.
58. Yamato, M. and T. Okano, *[Nanosurface modification by grafting temperature-responsive polymers]*. *Tanpakushitsu Kakusan Koso*, 2003. **48**(11 Suppl): p. 1602-1608.
59. Kano, M. and E. Kokufuta, *On the temperature-responsive polymers and gels based on N-propylacrylamides and N-propylmethacrylamides*. *Langmuir*, 2009. **25**(15): p. 8649-8655.
60. Asplund, B., J. Sperens, T. Mathisen, et al., *Effects of hydrolysis on a new biodegradable co-polymer*. *J Biomater Sci Polym Ed*, 2006. **17**(6): p. 615-630.
61. Sanders, W.T., G. Zeeman, and G. Lettinga, *Hydrolysis kinetics of dissolved polymer substrates*. *Water Sci Technol*, 2002. **45**(10): p. 99-104.
62. Kaur, B., S.P. McBride, A. Paul, et al., *Hydrolysis of p-nitrophenyl esters promoted by semifluorinated quaternary ammonium polymer latexes and films*. *Langmuir*, 2010. **26**(20): p. 15779-15785.
63. Iimura, S., K. Manabe, and S. Kobayashi, *Hydrophobic polymer-supported catalyst for organic reactions in water: acid-catalyzed hydrolysis of thioesters and transprotection of thiols*. *Org Lett*, 2003. **5**(2): p. 101-103.
64. Cui, Z., B.H. Lee, and B.L. Vernon, *New hydrolysis-dependent thermosensitive polymer for an injectable degradable system*. *Biomacromolecules*, 2007. **8**(4): p. 1280-1286.
65. Phaneuf, M.D., W.C. Quist, F.W. LoGerfo, et al., *Chemical and physical characterization of a novel poly(carbonate urea) urethane surface with protein crosslinker sites*. *J Biomater Appl*, 1997. **12**(2): p. 100-120.
66. Slutter, B. and W. Jiskoot, *Dual role of CpG as immune modulator and physical crosslinker in ovalbumin loaded N-trimethyl chitosan (TMC) nanoparticles for nasal vaccination*. *J Control Release*, 2010. **148**(1): p. 117-121.

67. Maitz, M.F., U. Freudenberg, M.V. Tsurkan, et al., *Bio-responsive polymer hydrogels homeostatically regulate blood coagulation*. Nat Commun, 2013. **4**: p. 2168.
68. Gao, X., Y. Cao, X. Song, et al., *Biodegradable, pH-Responsive Carboxymethyl Cellulose/Poly(Acrylic Acid) Hydrogels for Oral Insulin Delivery*. Macromol Biosci, 2014. **14**(4): p. 565-575.
69. Khutoryanskaya, O.V., Z.A. Mayeva, G.A. Mun, et al., *Designing temperature-responsive biocompatible copolymers and hydrogels based on 2-hydroxyethyl(meth)acrylates*. Biomacromolecules, 2008. **9**(12): p. 3353-3361.
70. Sheppard, N.F., Jr., M.J. Lesho, R.C. Tucker, et al., *Electrical conductivity of pH-responsive hydrogels*. J Biomater Sci Polym Ed, 1997. **8**(5): p. 349-362.
71. Schoener, C.A. and N.A. Peppas, *pH-responsive hydrogels containing PMMA nanoparticles: an analysis of controlled release of a chemotherapeutic conjugate and transport properties*. J Biomater Sci Polym Ed, 2013. **24**(9): p. 1027-1040.
72. Mohd Amin, M.C., N. Ahmad, M. Pandey, et al., *Stimuli-responsive bacterial cellulose-g-poly(acrylic acid-co-acrylamide) hydrogels for oral controlled release drug delivery*. Drug Dev Ind Pharm, 2013.
73. Gallagher, S., L. Florea, K.J. Fraser, et al., *Swelling and Shrinking Properties of Thermo-Responsive Polymeric Ionic Liquid Hydrogels with Embedded Linear pNIPAAm*. Int J Mol Sci, 2014. **15**(4): p. 5337-5349.
74. Hebeish, A., S. Farag, S. Sharaf, et al., *Thermal responsive hydrogels based on semi interpenetrating network of poly(NIPAm) and cellulose nanowhiskers*. Carbohydr Polym, 2014. **102**: p. 159-166.
75. Brassinne, J., J.P. Bourgeois, C.A. Fustin, et al., *Thermo-responsive properties of metallo-supramolecular block copolymer micellar hydrogels*. Soft Matter, 2014. **10**(17): p. 3086-3092.
76. Fell, H.B., *The effect of environment on skeletal tissue in culture*. Embryologia (Nagoya), 1969. **10**(3): p. 181-205.
77. Channing, C.P., *Influences of the in vivo and in vitro hormonal environment upon luteinization of granulosa cells in tissue culture*. Recent Prog Horm Res, 1970. **26**: p. 589-622.
78. Auersperg, N. and H. Erber, *Effects of tissue culture environment on growth patterns and ultrastructure of poorly differentiated human cervical carcinomas*. J Natl Cancer Inst, 1976. **57**(5): p. 981-994.
79. Shay, J.W. and W.E. Wright, *Tissue culture as a hostile environment: identifying conditions for breast cancer progression studies*. Cancer Cell, 2007. **12**(2): p. 100-101.
80. Nagwekar, J.B. and N. Muangnoicharoen, *Influence of temperature and nature of hydrophobic groups on thermodynamic parameters of hydrophobic bonding in a model polymeric system and their implications in drug-biopolymer interactions*. J Pharm Sci, 1973. **62**(9): p. 1439-1444.
81. Viswanathan, G., S. Murugesan, V. Pushparaj, et al., *Preparation of biopolymer fibers by electrospinning from room temperature ionic liquids*. Biomacromolecules, 2006. **7**(2): p. 415-418.

82. Dreher, M.R., W. Liu, C.R. Michelich, et al., *Thermal cycling enhances the accumulation of a temperature-sensitive biopolymer in solid tumors*. *Cancer Res*, 2007. **67**(9): p. 4418-4424.
83. Inbaraj, B.S., C.P. Chiu, G.H. Ho, et al., *Effects of temperature and pH on adsorption of basic brown 1 by the bacterial biopolymer poly(gamma-glutamic acid)*. *Bioresour Technol*, 2008. **99**(5): p. 1026-1035.
84. Xu, L.C., V. Vadillo-Rodriguez, and B.E. Logan, *Residence time, loading force, pH, and ionic strength affect adhesion forces between colloids and biopolymer-coated surfaces*. *Langmuir*, 2005. **21**(16): p. 7491-7500.
85. Horkay, F., P.J. Basser, A.M. Hecht, et al., *Insensitivity to salt of assembly of a rigid biopolymer aggrecan*. *Phys Rev Lett*, 2008. **101**(6): p. 068301.
86. Liu, S., N.H. Low, and M.T. Nickerson, *Effect of pH, salt, and biopolymer ratio on the formation of pea protein isolate-gum arabic complexes*. *J Agric Food Chem*, 2009. **57**(4): p. 1521-1526.
87. Pirzer, T., M. Geisler, T. Scheibel, et al., *Single molecule force measurements delineate salt, pH and surface effects on biopolymer adhesion*. *Phys Biol*, 2009. **6**(2): p. 025004.
88. Inbaraj, B.S., C.P. Chiu, Y.T. Chiu, et al., *Effect of pH on binding of mutagenic heterocyclic amines by the natural biopolymer poly(gamma-glutamic acid)*. *J Agric Food Chem*, 2006. **54**(17): p. 6452-6459.
89. Horkay, F., P.J. Basser, A.M. Hecht, et al., *Counterion and pH-Mediated Structural Changes in Charged Biopolymer Gels*. *Macromol Symp*, 2010. **291-292**(1): p. 354-361.
90. Luo, J., G. Giguere, and X.X. Zhu, *Asymmetric poly(ethylene glycol) star polymers with a cholic acid core and their aggregation properties*. *Biomacromolecules*, 2009. **10**(4): p. 900-906.
91. Deng, L., H. Qi, C. Yao, et al., *Investigation on the properties of methoxy poly(ethylene glycol)/chitosan graft co-polymers*. *J Biomater Sci Polym Ed*, 2007. **18**(12): p. 1575-1589.
92. Beauchamp, C.O., S.L. Gonias, D.P. Menapace, et al., *A new procedure for the synthesis of polyethylene glycol-protein adducts; effects on function, receptor recognition, and clearance of superoxide dismutase, lactoferrin, and alpha 2-macroglobulin*. *Anal Biochem*, 1983. **131**(1): p. 25-33.
93. Hariharan, V., S. Radhakrishnan, M. Parthibavarman, et al., *Synthesis of polyethylene glycol (PEG) assisted tungsten oxide (WO₃) nanoparticles for L-dopa bio-sensing applications*. *Talanta*, 2011. **85**(4): p. 2166-2174.
94. Gokarn, Y.R., M. McLean, and T.M. Laue, *Effect of PEGylation on protein hydrodynamics*. *Mol Pharm*, 2012. **9**(4): p. 762-773.
95. Lu, Y., S.E. Harding, A. Turner, et al., *Effect of PEGylation on the solution conformation of antibody fragments*. *J Pharm Sci*, 2008. **97**(6): p. 2062-2079.
96. Casettari, L., D. Vllasaliu, G. Mantovani, et al., *Effect of PEGylation on the Toxicity and Permeability Enhancement of Chitosan*. *Biomacromolecules*, 2010. **11**(11): p. 2854-2865.
97. Harris, J.M. and R.B. Chess, *Effect of pegylation on pharmaceuticals*. *Nat Rev Drug Discov*, 2003. **2**(3): p. 214-221.

98. Betancourt, T., J.D. Byrne, N. Sunaryo, et al., *PEGylation strategies for active targeting of PLA/PLGA nanoparticles*. J Biomed Mater Res A, 2009. **91**(1): p. 263-276.
99. Rissanen, S., M. Kumorek, H. Martinez-Seara, et al., *Effect of PEGylation on drug entry into lipid bilayer*. J Phys Chem B, 2014. **118**(1): p. 144-151.
100. Ellington, A.D. and J.W. Szostak, *In vitro selection of RNA molecules that bind specific ligands*. Nature, 1990. **346**(6287): p. 818-822.
101. Vaish, N.K., A.W. Fraley, J.W. Szostak, et al., *Expanding the structural and functional diversity of RNA: analog uridine triphosphates as candidates for in vitro selection of nucleic acids*. Nucleic Acids Res, 2000. **28**(17): p. 3316-3322.
102. Nieuwlandt, D., *In vitro selection of functional nucleic acid sequences*. Curr Issues Mol Biol, 2000. **2**(1): p. 9-16.
103. Lorsch, J.R. and J.W. Szostak, *In vitro selection of RNA aptamers specific for cyanocobalamin*. Biochemistry, 1994. **33**(4): p. 973-982.
104. Nieuwlandt, D., M. Wecker, and L. Gold, *In vitro selection of RNA ligands to substance P*. Biochemistry, 1995. **34**(16): p. 5651-5659.
105. Nutiu, R. and Y. Li, *In vitro selection of structure-switching signaling aptamers*. Angew Chem Int Ed Engl, 2005. **44**(7): p. 1061-1065.
106. Bock, L.C., L.C. Griffin, J.A. Latham, et al., *Selection of single-stranded DNA molecules that bind and inhibit human thrombin*. Nature, 1992. **355**(6360): p. 564-566.
107. Wang, K.Y., S.H. Krawczyk, N. Bischofberger, et al., *The tertiary structure of a DNA aptamer which binds to and inhibits thrombin determines activity*. Biochemistry, 1993. **32**(42): p. 11285-11292.
108. Bullock, T.L., L.D. Sherlin, and J.J. Perona, *Tertiary core rearrangements in a tight binding transfer RNA aptamer*. Nat Struct Biol, 2000. **7**(6): p. 497-504.
109. Buck, J., J. Noeske, J. Wohnert, et al., *Dissecting the influence of Mg²⁺ on 3D architecture and ligand-binding of the guanine-sensing riboswitch aptamer domain*. Nucleic Acids Res, 2010. **38**(12): p. 4143-4153.
110. Jiang, F., R. Fiala, D. Live, et al., *RNA folding topology and intermolecular contacts in the AMP-RNA aptamer complex*. Biochemistry, 1996. **35**(40): p. 13250-13266.
111. Al-Hashimi, H.M., A. Gorin, A. Majumdar, et al., *Alignment of the HTLV-I Rex peptide bound to its target RNA aptamer from magnetic field-induced residual dipolar couplings and intermolecular hydrogen bonds*. J Am Chem Soc, 2001. **123**(13): p. 3179-3180.
112. Zhao, X.Q., J. Wu, J.H. Liang, et al., *Single-molecule force spectroscopic studies on intra- and intermolecular interactions of G-quadruplex aptamer with target Shp2 protein*. J Phys Chem B, 2012. **116**(37): p. 11397-11404.
113. Kumar, N. and S. Maiti, *Quadruplex to Watson-Crick duplex transition of the thrombin binding aptamer: a fluorescence resonance energy transfer study*. Biochem Biophys Res Commun, 2004. **319**(3): p. 759-767.
114. Baque, M., A. Le Postollec, C. Ravelet, et al., *Investigation of low-energy proton effects on aptamer performance for astrobiological applications*. Astrobiology, 2011. **11**(3): p. 207-211.

115. Anthony, P.C., C.F. Perez, C. Garcia-Garcia, et al., *Folding energy landscape of the thiamine pyrophosphate riboswitch aptamer*. Proc Natl Acad Sci U S A, 2012. **109**(5): p. 1485-1489.
116. Tammela, T., B. Enholm, K. Alitalo, et al., *The biology of vascular endothelial growth factors*. Cardiovasc Res, 2005. **65**(3): p. 550-563.
117. Roy, H., S. Bhardwaj, and S. Yla-Herttuala, *Biology of vascular endothelial growth factors*. FEBS Lett, 2006. **580**(12): p. 2879-2887.
118. Yla-Herttuala, S., T.T. Rissanen, I. Vajanto, et al., *Vascular endothelial growth factors: biology and current status of clinical applications in cardiovascular medicine*. J Am Coll Cardiol, 2007. **49**(10): p. 1015-1026.
119. Mac Gabhann, F. and A.S. Popel, *Systems biology of vascular endothelial growth factors*. Microcirculation, 2008. **15**(8): p. 715-738.
120. Lee, I., K.Y. Yoon, C.M. Kang, et al., *Evaluation of the angiogenesis inhibitor KR-31831 in SKOV-3 tumor-bearing mice using (64)Cu-DOTA-VEGF(121) and microPET*. Nucl Med Biol, 2012. **39**(6): p. 840-846.
121. Potty, A.S., K. Kourentzi, H. Fang, et al., *Biophysical characterization of DNA and RNA aptamer interactions with hen egg lysozyme*. Int J Biol Macromol, 2011. **48**(3): p. 392-397.
122. Kanakaraj, I., W.H. Chen, M. Poongavanam, et al., *Biophysical characterization of VEGF-aHt DNA aptamer interactions*. Int J Biol Macromol, 2013. **57**: p. 69-75.
123. Shi, Y., H. Dai, Y. Sun, et al., *Fluorescent sensing of cocaine based on a structure switching aptamer, gold nanoparticles and graphene oxide*. Analyst, 2013. **138**(23): p. 7152-7156.
124. Ng, E.W., D.T. Shima, P. Calias, et al., *Pegaptanib, a targeted anti-VEGF aptamer for ocular vascular disease*. Nat Rev Drug Discov, 2006. **5**(2): p. 123-132.
125. Nutiu, R. and Y. Li, *Aptamers with fluorescence-signaling properties*. Methods, 2005. **37**(1): p. 16-25.
126. Carrasquilla, C., Y. Xiao, C.Q. Xu, et al., *Enhancing sensitivity and selectivity of long-period grating sensors using structure-switching aptamers bound to gold-doped macroporous silica coatings*. Anal Chem, 2011. **83**(20): p. 7984-7991.
127. Zhang, Y., B. Li, C. Yan, et al., *One-pot fluorescence detection of multiple analytes in homogenous solution based on noncovalent assembly of single-walled carbon nanotubes and aptamers*. Biosens Bioelectron, 2011. **26**(8): p. 3505-3510.
128. Cruz-Toledo, J., M. McKeague, X. Zhang, et al., *Aptamer Base: a collaborative knowledge base to describe aptamers and SELEX experiments*. Database (Oxford), 2012. **2012**: p. bas006.
129. Stoltenburg, R., C. Reinemann, and B. Strehlitz, *SELEX--a (r)evolutionary method to generate high-affinity nucleic acid ligands*. Biomol Eng, 2007. **24**(4): p. 381-403.
130. !!! INVALID CITATION !!!
131. Claffey, K.P., D.R. Senger, and B.M. Spiegelman, *Structural requirements for dimerization, glycosylation, secretion, and biological function of VPF/VEGF*. Biochim Biophys Acta, 1995. **1246**(1): p. 1-9.

132. Brandner, B., R. Kurkela, P. Vihko, et al., *Investigating the effect of VEGF glycosylation on glycosaminoglycan binding and protein unfolding*. *Biochem Biophys Res Commun*, 2006. **340**(3): p. 836-839.
133. Chassaing, S., A. Sani Souna Sido, A. Alix, et al., "*Click chemistry*" in zeolites: *copper(I) zeolites as new heterogeneous and ligand-free catalysts for the Huisgen [3+2] cycloaddition*. *Chemistry*, 2008. **14**(22): p. 6713-6721.
134. Wu, P., A.K. Feldman, A.K. Nugent, et al., *Efficiency and fidelity in a click-chemistry route to triazole dendrimers by the copper(i)-catalyzed ligation of azides and alkynes*. *Angew Chem Int Ed Engl*, 2004. **43**(30): p. 3928-3932.
135. Diaz, D.D., K. Rajagopal, E. Strable, et al., "*Click*" chemistry in a supramolecular environment: *stabilization of organogels by copper(I)-catalyzed azide-alkyne [3 + 2] cycloaddition*. *J Am Chem Soc*, 2006. **128**(18): p. 6056-6057.
136. Presolski, S.I., V.P. Hong, and M.G. Finn, *Copper-Catalyzed Azide-Alkyne Click Chemistry for Bioconjugation*. *Curr Protoc Chem Biol*, 2011. **3**(4): p. 153-162.
137. Mohanty, N., I. Vass, and S. Demeter, *Copper Toxicity Affects Photosystem II Electron Transport at the Secondary Quinone Acceptor, Q(B)*. *Plant Physiol*, 1989. **90**(1): p. 175-179.
138. Aston, N.S., N. Watt, I.E. Morton, et al., *Copper toxicity affects proliferation and viability of human hepatoma cells (HepG2 line)*. *Hum Exp Toxicol*, 2000. **19**(6): p. 367-376.
139. Arredondo, M., V. Cambiazo, L. Tapia, et al., *Copper overload affects copper and iron metabolism in Hep-G2 cells*. *Am J Physiol Gastrointest Liver Physiol*, 2004. **287**(1): p. G27-32.
140. Baskin, J.M., J.A. Prescher, S.T. Laughlin, et al., *Copper-free click chemistry for dynamic in vivo imaging*. *Proc Natl Acad Sci U S A*, 2007. **104**(43): p. 16793-16797.
141. Chargaff, E. and H.S. Shapiro, *Remarks on deoxyribonuclease*. *Exp Cell Res*, 1955(Suppl 3): p. 64-71.
142. Manchester, K.L., *Historical opinion: Erwin Chargaff and his 'rules' for the base composition of DNA: why did he fail to see the possibility of complementarity?* *Trends Biochem Sci*, 2008. **33**(2): p. 65-70.
143. Taberner, L., J. Bella, and C. Aleman, *Hydrogen bond geometry in DNA-minor groove binding drug complexes*. *Nucleic Acids Res*, 1996. **24**(17): p. 3458-3466.
144. Leo, A.J., *Evaluating hydrogen-bond donor strength*. *J Pharm Sci*, 2000. **89**(12): p. 1567-1578.
145. Wu, Z., A. Ono, M. Kainosho, et al., *H...N hydrogen bond lengths in double stranded DNA from internucleotide dipolar couplings*. *J Biomol NMR*, 2001. **19**(4): p. 361-365.
146. Dong, H., W. Hua, and S. Li, *Estimation on the individual hydrogen-bond strength in molecules with multiple hydrogen bonds*. *J Phys Chem A*, 2007. **111**(15): p. 2941-2945.
147. Spillman, W.B., Jr., R. Asmatulu, C.F. Jullian, et al., *Preliminary dielectric measurement and analysis protocol for determining the melting temperature and binding energy of short sequences of DNA in solution*. *Biotechnol J*, 2008. **3**(2): p. 252-263.

148. Tohl, J. and W. Eimer, *Interaction of a G-DNA quadruplex with mono- and divalent cations. A force field calculation.* Biophys Chem, 1997. **67**(1-3): p. 177-186.
149. Eriksson, M., F. Westerlund, M. Mehmedovic, et al., *Comparing mono- and divalent DNA groove binding cyanine dyes -- binding geometries, dissociation rates, and fluorescence properties.* Biophys Chem, 2006. **122**(3): p. 195-205.
150. Owczarzy, R., P.M. Vallone, F.J. Gallo, et al., *Predicting sequence-dependent melting stability of short duplex DNA oligomers.* Biopolymers, 1997. **44**(3): p. 217-239.
151. Owczarzy, R., Y. You, B.G. Moreira, et al., *Effects of sodium ions on DNA duplex oligomers: improved predictions of melting temperatures.* Biochemistry, 2004. **43**(12): p. 3537-3554.
152. Owczarzy, R., B.G. Moreira, Y. You, et al., *Predicting stability of DNA duplexes in solutions containing magnesium and monovalent cations.* Biochemistry, 2008. **47**(19): p. 5336-5353.
153. Owczarzy, R., A.V. Tataurov, Y. Wu, et al., *IDT SciTools: a suite for analysis and design of nucleic acid oligomers.* Nucleic Acids Res, 2008. **36**(Web Server issue): p. W163-169.
154. Owczarzy, R., *Melting temperatures of nucleic acids: discrepancies in analysis.* Biophys Chem, 2005. **117**(3): p. 207-215.
155. Owczarzy, R., I. Dunietz, M.A. Behlke, et al., *Thermodynamic treatment of oligonucleotide duplex-simplex equilibria.* Proc Natl Acad Sci U S A, 2003. **100**(25): p. 14840-14845.
156. Deniz, A.A., M. Dahan, J.R. Grunwell, et al., *Single-pair fluorescence resonance energy transfer on freely diffusing molecules: observation of Forster distance dependence and subpopulations.* Proc Natl Acad Sci U S A, 1999. **96**(7): p. 3670-3675.
157. Gryczynski, I., W. Wiczk, M.L. Johnson, et al., *Resolution of end-to-end distance distributions of flexible molecules using quenching-induced variations of the Forster distance for fluorescence energy transfer.* Biophys J, 1988. **54**(4): p. 577-586.
158. Parkhurst, L.J., *Distance parameters derived from time-resolved Forster resonance energy transfer measurements and their use in structural interpretations of thermodynamic quantities associated with protein-DNA interactions.* Methods Enzymol, 2004. **379**: p. 235-262.
159. Zheng, J., K. Liu, D.H. Reneker, et al., *Post-assembly derivatization of electrospun nanofibers via strain-promoted azide alkyne cycloaddition.* J Am Chem Soc, 2012. **134**(41): p. 17274-17277.
160. Zhu, J., C. Tang, K. Kottke-Marchant, et al., *Design and synthesis of biomimetic hydrogel scaffolds with controlled organization of cyclic RGD peptides.* Bioconjug Chem, 2009. **20**(2): p. 333-339.